Tampere University

Matteo Fè

RF BEAMFORMING IN VERY WIDEBAND RADIO SYSTEMS

Analysis of the beam squint problem

Faculty of Information Technology and Communication Sciences
Thesis type
Profs.: Mikko Valkama
Jukka Talvitie
December 2020

ABSTRACT

Matteo Fè: RF beamforming in very wideband radio systems
Thesis type
Tampere University
Electrical Engineering
December 2020

In the last few years the wireless data traffic has been encountered an extremely fast growth with a consequent high demand for accessible radio spectrum. In particular, the fifth-generation (5G) wireless technologies require much more resources in order to be able to satisfy the requirements of high data rates, low latency and high-capacity.In order to satisfy all these requirements it is necessary to look forward new resources that were not utilized before, like the mmWave spectrum. The frequency bands characterized by wavelengths in the order of millimeters are usually referred to as mmWave frequencies. They include all the frequencies between 30GHz and 300GHz. These frequencies can be utilized in a very efficient way through techniques like beamforming, which will allow us to obtain the best effort from the new spectrum available. The main problem of the 5G generation is that the signal received from the arrays will result in the sum of many delayed components of the original signal which usually are approximated as phase shifts. Due to the very large bandwidth available in the mmWaves, it will not be possible to neglect anymore the delays and thus the phased-arrays will be characterized by a frequency dependency. This effect is referred to as beam squint.

In this work the effects caused by the beam squint are studied for the cases of uniform linear array (ULA), uniform planar array (UPA) and uniform circular array (UCA). The simulations show that the different array configurations are not affected in the same way by the beam squint problem due to their different characteristics. In particular, it has been shown that the linear geometry is the most affected by the beam squint. Finally, in order to study the impact on the transmission of a signal, it was performed a simulation of an OFDM transmission characterized by an analog beamforming architecture under the beam squint phenomenon. The results have confirmed that beam squint decreases the channel capacity, and therefore, it should be taken into consideration both for path selection and channel estimation.

Keywords: Antenna arrays, Beamforming, Beam squint, MIMO, mmWave, Wideband, 5G

CONTENTS

LIST OF FIGURES

LIST OF TABLES

LIST OF SYMBOLS AND ABBREVIATIONS

Φ	Propagation delay
δ	Phase shift
λ	Wavelength
ϕ	Azimuth angle
θ	Elevation angle
a	Radius of the circular array
ADC	Analog-to-Digital Converter
AoA	Angle of arrival
AoD	Angle of departure
BW	Bandwidth
CBW	Channel Bandwidth
CSI	Channel State Information
d	Distance between two adjacent antennas in a uniform array
DAC	Digital-to-Analog Converter
DFT	Discrete Fourier Transform
DSA	Dynamic spectrum access
f	Frequency
FD	Fractional delay
FFT	Fast Fourier Transform
G	Gain
HPBW	Half power beamwidth
IDFT	Inverse discrete Fourier Transform
IFFT	Inverse Fast Fourier Transform
k	Wavenumber
LOS	Line of sight
MIMO	Multiple input multiple output
OFDM	Orthogonal Frequency Division Multiplexing
PDP	Power delay profile
SCS	Subcarrier spacing

SNR	Signal to Noise Ratio
TAU	Tampere University
TUNI	Tampere Universities
UCA	Uniform Circular Array
ULA	Uniform Linear Array
UPA	Uniform Planar Array

1 INTRODUCTION

In the last decades the applications of wireless technologies have been experiencing unprecedented growth with a significant increase also in the number of devices connected. As can be seen from figure 1.1, this trend is supposed to increase even more in the following years with an estimated number of connected users of 8.9 billion in 2025 and with a consequent request of new resources to satisfy all the demands. In this scenario it is extremely important to develop a new generation of wireless communications technologies.
The 5G generation of mobile communications will enhance the main specifications of the current communication systems by offering higher data rates (up to 20Gbps) and lower latency. The new generation will also extend the areas of interest for the mobile communications in order to develop new utilization such as automotive, connected devices and others. In order to enhance the spectrum access it is possible to reuse the non-utilized spectrum through dynamic spectrum access (DSA) or to move forward new frequencies band such as the millimeter-wave (mm-Wave) bands.
Until now, most of the wireless communications have been using the frequency band in the range of 300MHz-6GHz. The new generation, instead, opens the boarders towards a new part of the frequency spectrum, the one of the mm-waves. With the term mm-Waves it is referred the frequency spectrum from 30GHz up to 300GHz, but sometimes also the frequencies between 20GHz and 30GHz are included.

The frequency spectrum beyond 52.6GHz is of particular interest allowing for faster data speeds and much higher bandwidth than ever before. A particular interest has been shown especially for the the frequency ranges above 50 GHz due to the fact that they offer a very large frequency spectrum available with very large bandwidths. Moving to higher frequency is definitely an easy way to utilize more efficiently the frequency spectrum, but it also introduces some difficult challenges. In particular such small wavelength is extremely affected by the propagation loss due to high atmospheric absorption, there is a much higher phase noise, the power amplifiers are not to efficient due to nonlinearities and strict requirments regarding the power spectral density are present, compared to the sub-30 GHz bands.

The mm-wave communication systems can accomplish extremely high data rates but at the same time they introduce problems that were not present before regarding the component electronics used in the systems. In fact, components such as power amplifiers, low noise amplifiers, mixers and antennas are too big in size and consume too much

power to be applicable in mobile communication [2].

Until now, the global wireless communications have been using the radio spectrum in the frequency band under 6 GHz. The main benefit of the mm-wave is that the entire bandwidth that has been used for the previous generations easily fits within the bandwidth of the single 60 GHz unlicensed band [3], and even spectrum will remain available in the higher frequencies.

In the mmWave bands there is a lot of spectrum available, but it also introduces new challenges in the propagation system.

First of all, the effective communication distance is limited by a more sever signal attenuation compared to microwave signals and thus reduces the cell radius. On the other hand, line-of-sight (LOS) propagation can help to reduce significantly the co-channel interference by the employment of highly directional antennas. This introduces new challenges in the design of hardware components, such as very directive antennas, high density antenna arrays and power amplifiers with large dynamic ranges [4]. Very often one of the main problem is that the size and the power required by the systems used in these applications exceed the limits applicable for mobile communications. This is why new techniques to increase the transmitted power and to improve the directivity are needed. One technique used for this purpose is the beamforming, which consists in controlling the signal amplitude and phased both in the transmission and reception mode. With this technique it is also possible to obtain spatial selectivity by adapting the radiation patterns of the devices involved in the communication in an optimal way.

It is possible to compensate for those attenuation by using antenna arrays with an higher number of elements and directing their beams towards the desired direction by using the beamforming techniques. The compact arrays resulting from small wavelengths can be friendly to mobile application [5].

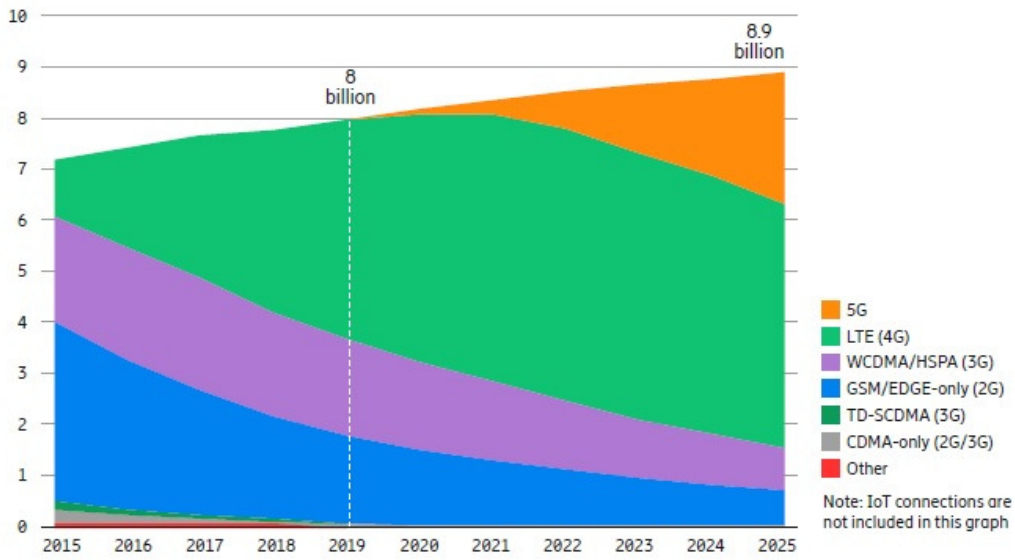

Figure 1.1. *Mobile subscription by technology [1]*

Moreover, that short wavelengths introduced by the frequency bands adopted are allowing the integration of a very high number of radiating elements in a reduced surface, which will help to compensate better for the higher attenuation introduced.

The new communications will need take advantage from the rapid changes of the wireless channel because antenna array with higher gain will be used to overcome the higher attenuations. The rapid variations to which the signal will be subjected need to be predicted in order to design properly channel state feedback algorithms and to use the most appropriated techniques for link adaptation and tracking of the channel.

The aim of the beamforming technique is to focus the energy of the signal towards the desired used, in order to avoid any dispersion of the power. The beamforming techniques basically consist on modelling in a precise way the amplitude and the phase of the signals in such a way that they will combine coherently towards the desired target and incoherently in the undesired directions. This will help to cover only the region of the cells where the signal is needed. For massive MIMO antennas beamforming algorithms can be used in order to predict the path for reaching the end user by undergoing the lowest possible attenuation. This will help to aviod interference and to improve the data rate and spectral efficiency of the communications. Modern communication systems utilize smart antenna systems which are able to merge the benefits deriving from having high arrays and diversity gain. Is such a way it is possible to reduce the channel interference, resulting in an increase of the capacity of the communication link. The mentioned techniques can be accomplished by steering the signals transmitted by the antenna array. The beamforming can be applied in both the transmitter and receiver schemes. In the first case, it can be developed between the signal source and the antennas of the array, in order to focus the power of the signal towards the receiver location in the space. This procedure is referred to as transmit beamforming. In the receiving chain, instead, it is common to implement the beamforming techniques right after the antenna array. This techniques is the so called receive beamforming.

In order to underline the importance of having very high antenna gains when operating in these new frequency bands, typical link budgets for millimeter wave systems are presented in the 1.1 in the case the transmission is taking place in the open-air or inside a building.

The usage of new techniques such as beamforming helps to achieve the desired results in terms of available bandwidth, transmission rate ecc... The 60 GHz band has been tested by using extremely simple analog beamforming methods, which have shown good results only for short range indoor communications. Unfortunately these results may also introduce new challenges that come out in order to optimize the available resources. For examples, when having a very wideband signal it is possible to experiments transmission behaviours that were not expected to happen.

In the analog beamforming, the phase shifter used in the array are usually tuned to the carrier frequency of the signal, but apply to all the bandwidth. A phase shift can be

Table 1.1. *Common link budgets for millimiter wave communication both for open air and indoor[6]*

Parameter	Indoor	Outdoor	
Carrier Frequency (GHz)	60	28	72
Max. range(m)	10	1000	1000
Bandwidth (GHz)	2	0.5	0.5
Transmit Power(dBm)	10	25	25
Propagation Loss(dB)	-88	-122	-130
Additional Loss(dB)	00	-20	-20
Implementation Loss(dB)	-5	-5	-5
Thermal PSD (dBm/Hz)	-174	-174	-174
Rx Noise Figure(dB)	10	10	10
Rx. Thermal Noise (dB)	-71	-77	-77
Receiver SNR (dB)	-12	-45	-53
Required SNR (QPSK) (dB)	10	10	10
System Margin(dB)	-22	-55	-63
Transmit Antenna Gain (dBi)	20	40	40
Receive Antenna Gain (dBi)	10	20	25
System Margin (dB) with Tx and Rx Antenna Gains	**8**	**5**	**2**

used to fairly approximate a time delay if the signal bandwidth is small, but unfortunately this approximation is no longer valid when the bandwidth of the signal is much higher and when the angle of arrival (AoA) or angle of departure (AoD) are not close to the direction perpendicular to the array. This introduces a frequency dependency in the array response, which implies that different frequencies in the desired bandwidth will be "squint" as a function of the frequency. This phenomenon is called beam squint.

The effect of beam squint in the array are varying depending on different characteristics: the AoA/AoD, the channel bandwidth utilized and also the number of elements in the array.

In this thesis work the phenomenon of beam quint is introduced and its effects are studied. The beam squint is first modelled for the uniform linear array (ULA), uniform planar array (UPA) and uniform circular array (UCA). Its effects are taken into account by considering it in the channel model propagation. It is shown how the beam squint introduces a frequency dependency in the array gain which affects the maximum achievable gain of the array, and thus the capacity, on different frequencies. It is also studied how the effects of this problem are changing as a function of number of radiating elements in the array, of the channel bandwidth and of the desired AoA or AoD.

The radio link simulations were confirming what studied theoretically. In fact, a transmission under beam squint is affected by it and is showing a much lower transmission gain and very high losses especially on the edges of the considered frequency band.

The structure of this thesis is as follows. Chapter 2 provides a detailed background for the new challenges encountered when working in the mm-Waves. In particular, it is first discussed how higher path loss present for these waves is influencing the channel model. One solution for this problem is represented by using very large antenna arrays in order to be able to apply beamforming techniques. Thus, a short review of antenna arrays and beamforming schemes is presented. Chapter 3 introduces the phenomenon of the beams quint and its effects. In particular the models for beam squint for a ULA, UPA and UCA arrays are developed, resulting in a baseband-equivalent models that incorporate beam squint. Chapter 4 is studying the effects of the beam squint on a radio link simulation with OFDM waveform. Finally, chapter 5 summarizes the conclusions of this work and illustrates what are the possible directions for future research.

2 THEORETICAL BACKGROUND

In this chapter the propagation model that is encountered in mm-Wave communications is analyzed and compared to the sub-6G GHz radio channel. The difficulties introduced by the mm-Wave make necessary to utilize antenna arrays which allow to obtain a very high gain. This can be achieved in different ways, for example by using arrays with a very high number of elements or utilizing beamforming techniques. A short recap about antenna arrays is done in section 2.2.

Then, the concept of beamforming is introduced and the the state of art on mm-Wave beamforming is analyzed, with particular interest for the case of mm-Waves. Then the different beamforming architectures are discussed.

Finally, the problem of beam squint is introduced and its main challenges are briefly analyzed.

2.1 Channel model for mm-Wave communication

The wireless communication technologies preceding the fifth-generation are mostly working in the sub-6 GHz frequency band. 5G mmWave wireless channel bandwidths will be much wider compared to today's LTE. In fact LTE utilized 20MHz cellular channels, while the idea for 5G is to use up to ten times bigger channel bandwidth. This will significantly influence the wavelength shrink and thus it will be extremely important to understand and study how the signals will behave when subjected to greater attenuation due to diffraction and material penetration.

The radio propagation environment for frequencies over 52.6GHz generates also new challenges regarding the propagation of the signals. The mm-Waves in fact are more affected by path losses and will attenuate more due to atmospheric absorption. It should also be noticed that while signals with longer wavelengths can penetrate through buildings without being subjected to high attenuations, mmWave signals are not showing the same characteristics. Moreover, as can be seen from figure 2.1 at mm-waves frequencies the gaseous attenuation and weather start to have higher impact on the pathloss attenuation. The signals are thus very sensitive to the atmospheric attenuation. In particular, it can be noted that at 60GHz is present a very high peak of absorption due to O_2. The behaviour shown in the picture has to be taken into account only for long-range communication. Thus, it is possible to take advantage of the 60 GHz frequency band for short-range communications, enabling the development of heterogeneous network with microcells.

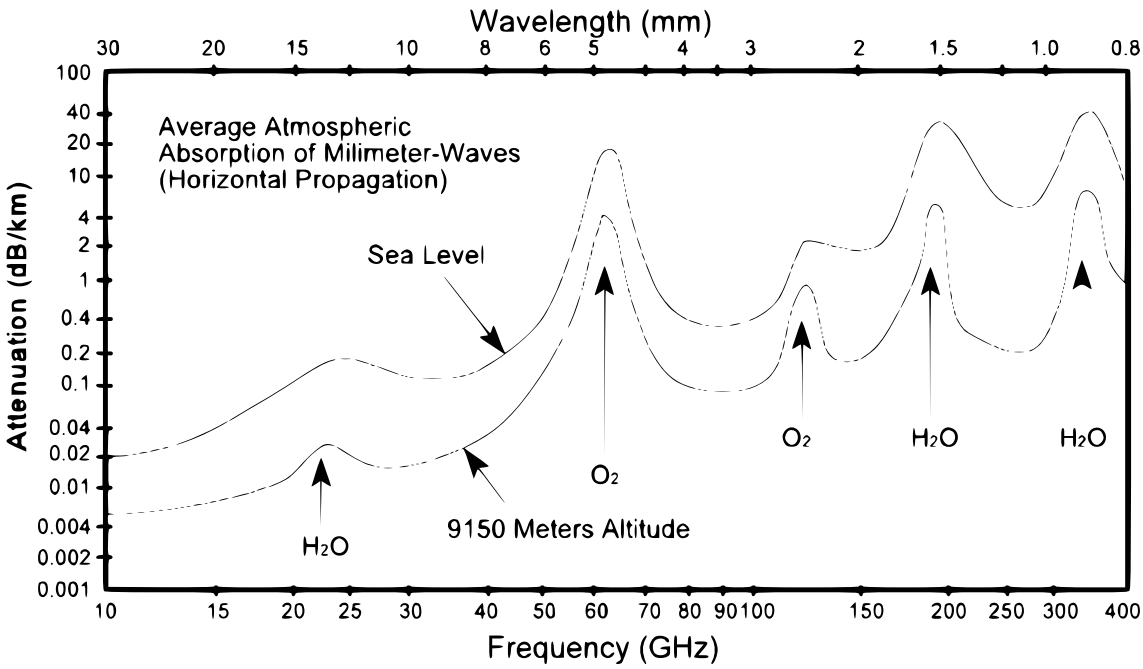

Figure 2.1. *Behaviour of the atmospheric attenuation as a function of frequency [7]*

Many times it is assumed that the effects of the path loss are directly proportional to the carrier frequency of the communication, but various studies made in different environments [8], [9], [10], have shown that according to Friis' equation this is correct only in the case when the gain of the radiating element is assumed constant over all the frequency band. On the other hand, if the physical size of the antenna (e.g., effective aperture) in not changing in the considered frequency band at both the transmitter and receiver sides, then path loss in free space actually decreases quadratically as frequency increases [11].

The new communications will need to take advantage of the rapid changes happening in the wireless channel and to exploit them in order to obtain an higher number of paths for communicating. The higher gain of each radiate element will help to compensate for the attenuation. Moreover, it should be considered that the lower wavelength will be more affected by the diffuse scattering even if they will propagate for shorter distances [11].

In this scenario, the environment around the two communicating systems can introduce large angular spread of incident waves on the receiving component, rich multipath components and penetration loss relatively low can penetrate through building walls and windows. Thus, in this case a distance dependent stochastic channel model is good enough to describe the channel propagation. As was shown in [12], the power-delay profile (PDP) of the channel is decreasing almost in a linear way with respect to the delay of of propagation. This is also shown in figure 2.2. Thus, it is possible to estimate quite easily the predicted loss in the propagation.

Usually at mm-waves the channel can be quite sparse and we do not have so many multipaths and the incoming path are only for certain angles. Usually there is a very strong LOS component and only few multipath components. This was also demonstrate in [13] and the results are presented in figure 2.3, were a LOS peak is present and also

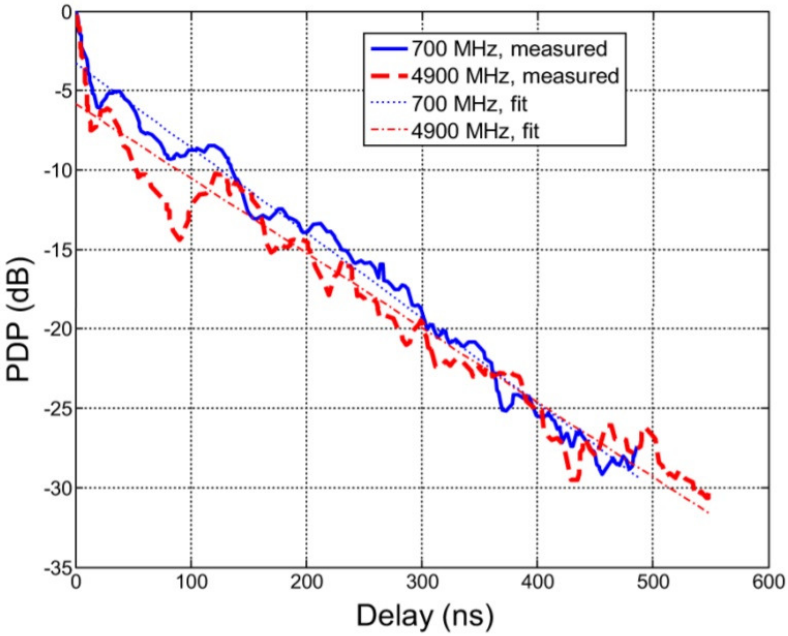

Figure 2.2. *Average PDP for 700- and 4900-MHz bands, all outdoor-indoor data [12]*

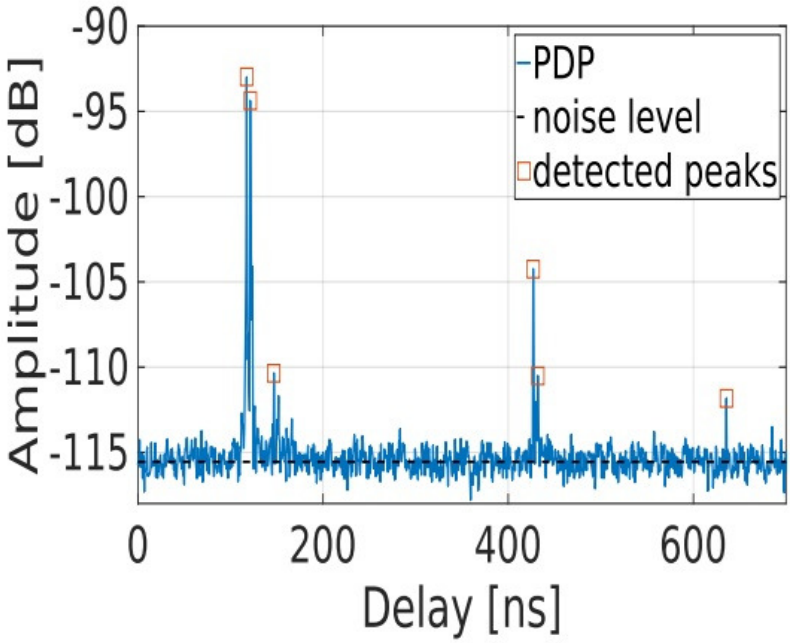

Figure 2.3. *PDP for a measured link at 32GHz [13]*

two multipath components can be seen. It is extremely important to notice that when the user moves the amplitude and the delays of these peaks are changing. Moreover, at mm-waves we are more sensitive to blockage due to high penetration loss of objects and reduced diffraction.

These problems were not present before because for lower frequencies the waves diffract more easily, instead when using higher frequencies the channel model is more sensitive

to the specific environment and this makes the stochastic models not so useful.

All these conditions imply that for mm-waves we need high gain for the antenna design and this can be achieved by utilizing antenna arrays. Moreover, in order to direct the main beam of the transmitter towards the desired direction, beam steering is needed.

It is extremely important to take into account the path loss the signal will encounter. An isotropic antenna radiates a power evenly in all the directions accordingly to the following expression:

$$S = \frac{P_t}{4\pi r^2} \tag{2.1}$$

which basically is the antenna transmission power divided by the spherical area. This power density is not affected by the frequency at all. This means that electromagnetic waves attenuate exactly in the same way for both low and high frequencies.

In order to receive the power of the electric field, also a receiving antenna is needed. The receiving antenna receives this power according to its effective aperture size

$$P_r = SA_e = \frac{P_t A_e}{4\pi r^2} \tag{2.2}$$

However, antenna gain is directly linked to the effective aperture of the antenna by the relation

$$A_e = \frac{G\lambda^2}{4\pi} \tag{2.3}$$

so the receiving power can be written as

$$P_r = \frac{P_t G_r \lambda^2}{(4\pi)^2 r^2} \tag{2.4}$$

With directional transmit antenna, the Friis formula applies and results in:

$$\frac{P_r}{P_t} = G_t G_r (\frac{\lambda}{4\pi r})^2 \tag{2.5}$$

expressed with aperture $P_r P_t = (\frac{A_t A_r}{r^2 \lambda^2})$.

We can notice that, if both RX and TX antenna are kept the same size the power transfer actually increases proportional to $\frac{1}{\lambda^2}$. For this reason it is actually beneficial to use high frequencies for point-to-point links.

Of course, we have also to remember that, even if the power transfer increases much, higher losses will be present.

2.2 Antenna arrays

In many applications it is necessary to have a very narrow pattern in a specific direction in order to reach high values of directivity, especially for long distance communications. Usually, it is not possible to reach these results by using a single antenna. Often antenna elements with larger dimensions will result in an higher directivity value, but it is not very practical to utilize antennas with big dimensions. That is the reason why, instead of using antennas with very large dimensions, it is better to use an assembly of smaller elements that will form the so-called antenna array.

The electromagnetic power radiated by the alignment of the antennas can be calculated by the geometrical sum of the vector of the field of each single antenna. This means that, in order to obtain patterns characterized by an high directivity, it is needed that the patterns of the single antenna will combine coherently towards the desired angle and destructively in the remaining space. The total pattern of the array can be influenced by many factors [14]:

1. The geometrical shape of the array
2. The distance between the elements
3. The amplitude of the excitation of the individual element
4. The phase of the excitation of the individual element
5. The pattern of the individual elements

2.2.1 Linear arrays

As demonstrated in [14], in order to make the design of the arrays much easier, the far-zone field of an array is the product of the element's pattern (usually positioned in the origin) and the array factor of that array. The array factor (AF) is calculated by substituting every single element with an isotropic antenna [14]:

$$\boldsymbol{E}(\textit{total}) = [\boldsymbol{E}(\textit{single element at reference point})] * [\textit{Array factor}] \tag{2.6}$$

It is usually referred to it as *pattern multiplication* and one example is depicted in 2.6.

Considering a linear array composed of N identical antennas excited with equal amplitude signals and a progressive phase delay of δ, the array factor can be express with the expression :

$$AF = \sum_{n=1}^{\infty} e^{-j(n-1)\psi} \tag{2.7}$$

where

$$\psi = kd\cos\theta + \delta. \tag{2.8}$$

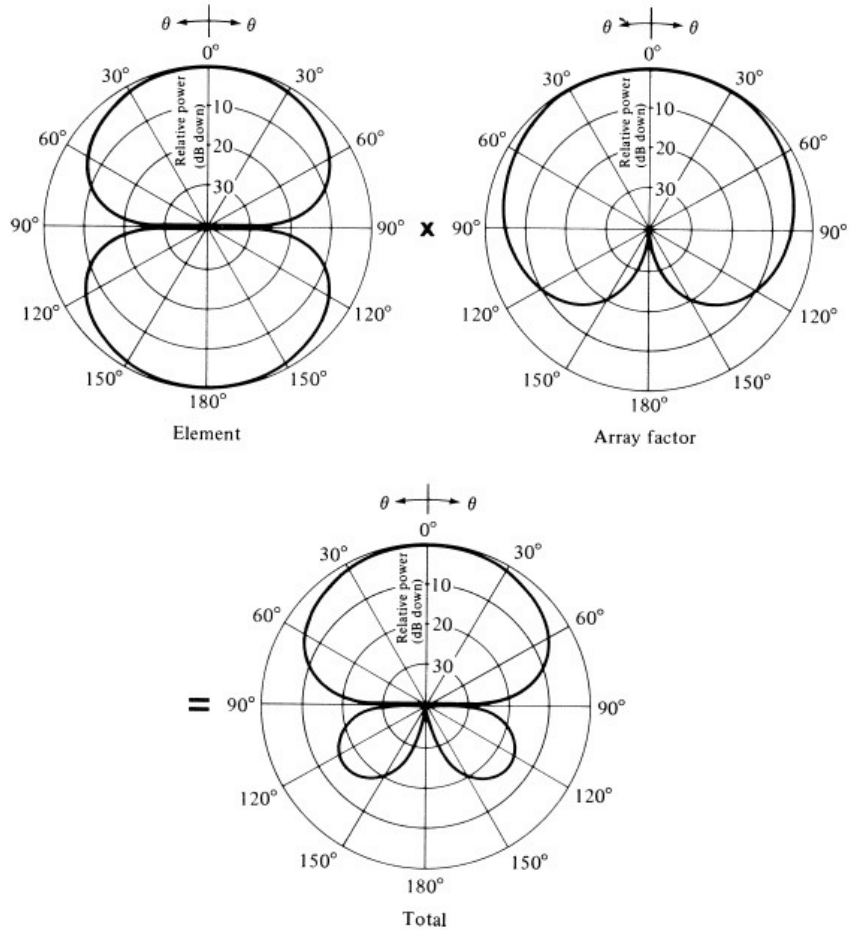

Figure 2.4. *Example of pattern multiplication [14])*

In this equation k is the wavenumber, d is the distance between the elements and θ is the angle between from where the signal is impinging the array.

The AF can be also written as:

$$AF = \left[\frac{\sin\left(\frac{N}{2}\psi\right)}{\sin\left(\frac{1}{2}\psi\right)}\right]. \tag{2.9}$$

The array factor is a function of ψ and is a Fourier series [14]. Since it is common to represent the polar plots as function of the angle θ, the nonlinear transformation from ψ to θ can be accomplished graphically. The function 2.9 can be easily plotted in rectangular coordinates. Then it is important to notice that it is a function of θ, thus it will be good to plot it in polar coordinates. In particular the expression of ψ is the equation of a circle which is centered in $\psi = \delta$ and has a radius of *kd* 2.8. The diameter of the circle defines the *visible region*. The distance between the antennas in the array expressed as function of wavelength, $\frac{d}{\lambda}$,is influencing the dimension of the circle and consequently also the amount of array factor appearing in the visible region. determines the size of the circle and thus how much of the array factor appears in the visible region. It is important to

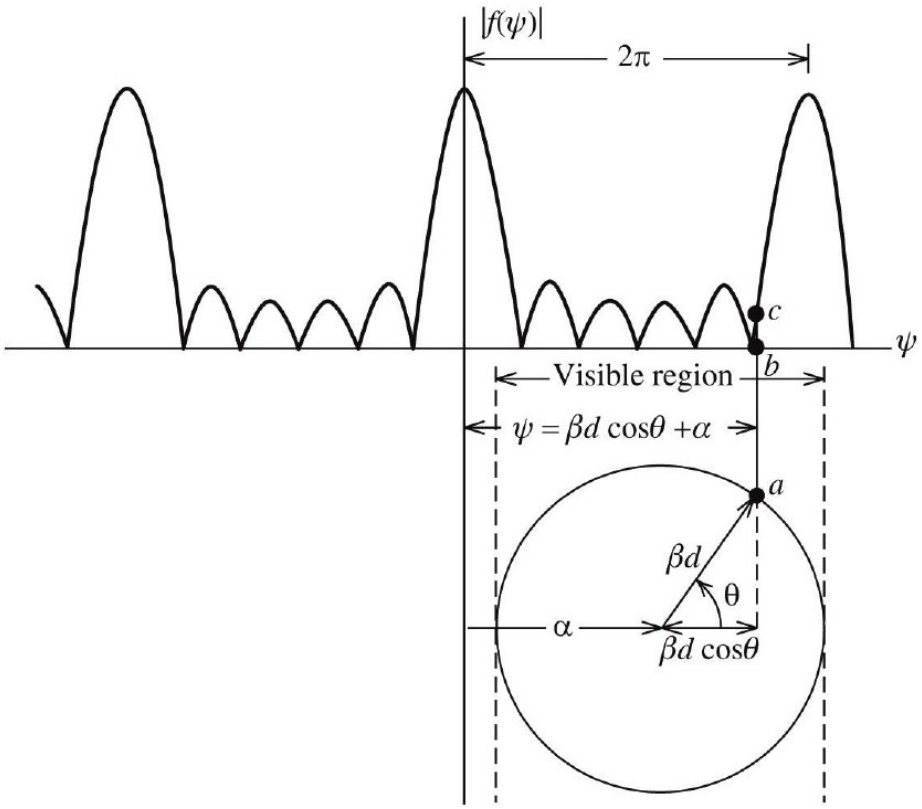

Figure 2.5. *Array factor derivation in polar coordinates θ [15]*

notice that when the antennas spacing is equal to $d = \lambda/2$ the visible region coincides with one period of the array factor. Figure 2.5 illustrates one example about how to plot graphically the array factor as a function of polar angle θ.

It is really interesting to notice that it is possible to obtain a tilt of the radiation pattern by changing the phase of the signals of every single antenna. This application is made possible thanks to the use of different phase excitation in each element. One method to obtain this result is to feed each antenna with a transmission line with a different length, because the time phase of the feeding signal is increasing with an increase of the length of the transmission line. When the array is linearly aligned, the main beam will be directed toward the direction

$$\theta_{max} = \arccos -\frac{1}{2\pi}\frac{\lambda_0}{d}\delta, \tag{2.10}$$

where δ is the phase shift between two consecutive radiators.

Knowing the desired direction where we would like to direct the maximum, the value of δ can be found by using the inverse formula

$$\delta = -d\frac{2\pi}{\lambda_0}\cos\theta_{max}. \tag{2.11}$$

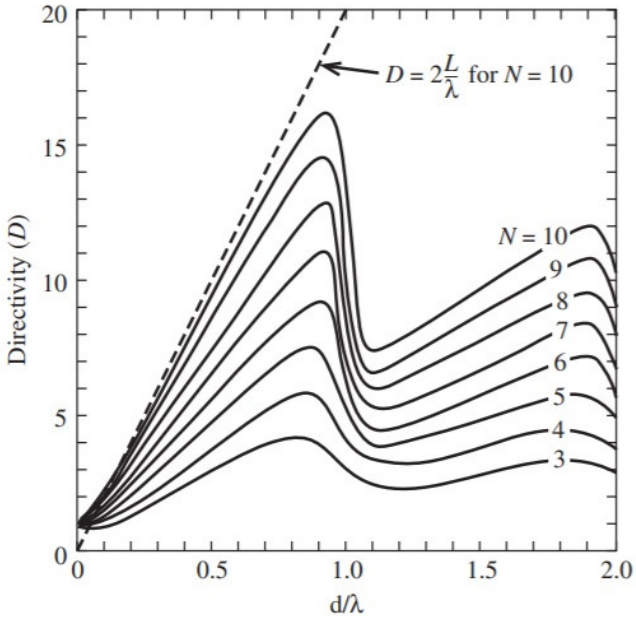

Figure 2.6. *Directivity as a function of element spacing for a broadside array of isotropic elements for several element numbers N [15]*

Once the phase shift is known, we will need to be very careful to control that no grating lobes will exist. Since in most of the cases the array factor present a sinusoidal dependence on the phase shift, it is possible to avoid the grating lobes by imposing that they will exist only for non real angles. The array pattern can be modelled by adding a phase shift such that $\delta(f) = 0$ at the desired direction. The desired difference of phase can be obtained either by the use of phase shifters, which produce a constant phase shift, or time delays, which produce a phase shift that is changing with frequency.

As we have seen until now, an element spacing lower than $\lambda/2$ ensures the absence of any grating lobe in the radiation diagram. On the other hand, there is a trade off between the directivity of the array and the element spacing. Figure 2.6 plots the behaviour of the directivity for arrays with different dimensions as a function of the spacing between the elements when is not present any phase shift between consecutive elements ($\beta = 0$). As it possible to notice the directivity tends to increase also for element spacing bigger than $\lambda/2$ and then it falls off steeply around one wavelength. This behaviour can be explained thanks to the fact that grating lobes are introduced in the visible region. A particular results is obtained when the distance between the elments is a multiple integer of a half-wavelength: the directivity is equal to the number of elements ($D = N$) for isotropic antennas and element spacing of $d = n\lambda/2$. Thus, we can conclude that for element spacing which are integer multiples of half wavelength the directivity is independent of the scan angle.

Many times arrays are designed in order to obtain the desired results by using the lowest possible number of radiating elements. Thus, sometimes the elements are spaced one wavelength apart each other. Referring to the figure 2.6 and considering what we

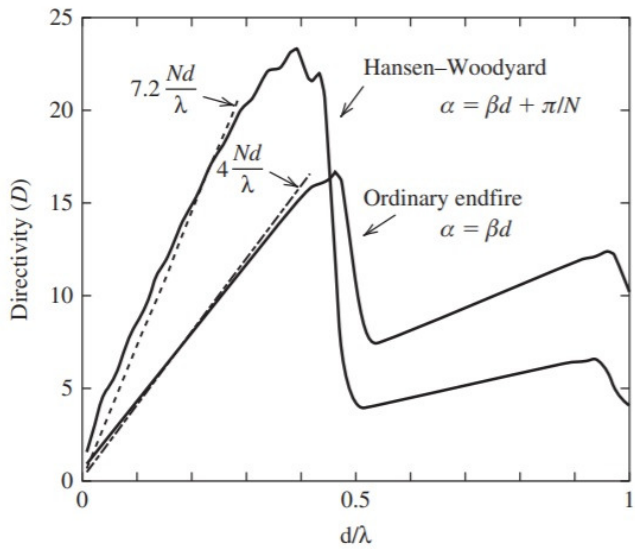

Figure 2.7. *Directivity as a function of element spacing for a endfire array of isotropic elements for several element numbers N [15]*

analysed in the previous paragraphs, we can conclude that the best trade-off between directivity and the presence of grating lobes can be achieved by using a broadside UE ESLA array where the distance between the elements has as upper limit one wavelength. The arrays are usually designed by considering a distance between their elements close to a wavelength. In this way it is possible to maintain low the number of antennas used and also to reduce the cost and complexity of the relative feeding network.

Array are often designed to have an element spacing near a wavelength to keep the number of elements as low as possible and to limit the cost and complexity of the antenna and associated feed network.

The directivity of the end-fire array as function of the distance between its elements is analysed in Fig. 2.7. Comparing the two graphs of figures 2.6 and 2.7, it is evident that broadside and endfire have very similar trends. In this case, the only difference is that the curves are falling off steeply around half wavelength. This behaviour can be explained thanks to appearance of grating lobes towards the endfire direction opposite the main beam.

From figure 2.7 it is immediate to notice that, given a certain number of elements, the Hansen-Woodyard array will achieve an higher directivity than any other endfire array. It is really important to notice that this is true only when using an element spacing lower than $\lambda/2$. In fact, after this value its directivity is much lower than all the other cases.

2.2.2 Planar arrays

Many applications require certain specifics that are not always obtainable by using linear arrays. For instance, it is possible to scan linear arrays only in the plane containing the line the antennas' centers. These limitations usually affect the realizable gain. Thus, in all the cases where linear arrays are not enough they are substituted by multidimensional arrays. This category of arrays can provide pencil beams, higher gain or the capability to scan the main beam towards the desired target. Multidimensional arrays are characterized by four main factors [15]:

1. The perimeter of the array
2. The shape of the surface on which the element centers are located
3. The lattice of the array
4. The phase of the excitation of the individual element

The pattern multiplication principles that was described in the previous section can be applied also for multidimensional arrays with similar elements. If we consider an array composed of equal antennas and with the same orientation, the resulting pattern can be factorized as shown in 2.7. It can be demonstrated that the array factor of a rectangular geometry on the xy plane can be obtained by the multiplication of the array factors of the linear arrays in the x- and y-directions. Also in this case the grating lobes will appear for element spacing higher than $\lambda/2$. Thus, to avoid them it is necessary to satisfy the same principles as in the linear case.

The directivity of a multidimensional array can be computed using the data from linear arrays. It is important to notice that the directivity of an arrays with two main lobe is the half of the directivity that we could obtain from the same array with only one lobe. To calculate the directivity there are different methods. It is possible to compute the directivity thanks to the formula provided in [15]:

$$D = \frac{4\pi}{\lambda^2} A_{cell}. \tag{2.12}$$

In the case of a planar array with a square lattice, the area of the cell is $A_{cell} = d_x d_y = (\lambda/2)(\lambda/2) = \lambda^2/4$ and yields $D_{cell} = \pi$. With the same procedure the directivity of a complete arrays can be found:

$$D_{Max} = \frac{4\pi}{\lambda^2} A_p = \pi D_x D_y \tag{2.13}$$

where A_p is the physical area of the full array.

Th right side of this formula is derived from using $A_p = L_x L_y$, where L_x and L_y are the sides of the area to cover, and introducing the directivities of uniform line sources in the x and y directions of a planar array in the xy-plane, where $D_x = 2L_x/\lambda$ and $D_y = 2L_y/\lambda$.

In most of the cases, the directivity has to be computed by using numerical integration methods.

2.3 Beamforming

In the previous paragraphs it was introduced one of the main characteristics of the 5G NR technologies, which is to utilize configurations with many antennas at both the sides of the communication link. In order to obtain the best benefit from these big arrays of antennas, it is necessary to utilize some beamforming techniques. The beamforming concept can be introduced by thinking that we are primarily working in terms of the directions angles and that the complete channel state information (CSI) of the instantaneous complex gain are not necessarily used. The capacity provided by available time/frequency resources can be divided in space (i.e. in physical environment). Thus, beamforming is one of the key technologies in modern and future wireless systems. On the TX side, the full or partial CSI based digital beamforming/spatial processing is commonly also called spatial precoding, while on the RX side it is referred to as spatial filtering.

With fairly simple spatial signal processing, we can create directional properties to the antenna system such that signal(s) from certain direction(s) are received well (combine coherently) while the signals from some other directions (angles) are suppressed (combine destructively). Besides directing the transmission/reception on the desired direction, it is also possible to reject certain directions. This can be beneficial to reduce interference of the system.

The beamforming technique is very useful because it enables to create space selectivity both in transmission and in reception. It is basically a spatial filter which can be used in combination with ordinary filtering and temporal signal processing. Directivity can be obtained by properly adjusting/observing the relative phases of the transmitted/received signal in separate antenna elements.

The beamforming concept is not used only in arrays of antennas, but can also be utilized for other applications, for example with arrays of microphones in the audio processing.

There are a lot of alternative optimization and design methods for the combiner weight in the literature. In general, for classical beamforming, we can conclude that the only channel knowledge needed is the direction of arrival AoA. The simplest beam-forming technique is the spatial matched filter. It is built on the assumed target angle θ_l and the corresponding steering vector $s(\Phi_l)$: the weights utilized in this case have unit amplitude and they are modifying the phase of the arriving signal. Thus, it is possible to conclude that the weights used are the complex conjugate of signal steering vector 2.14.

$$\mathbf{w}_{opt} = \frac{S(\Phi_l)}{\sqrt{(s(\Phi_l))^H s(\Phi_l)}} \tag{2.14}$$

This technique maximizes the total output variance under the constraint || **w**||=1.

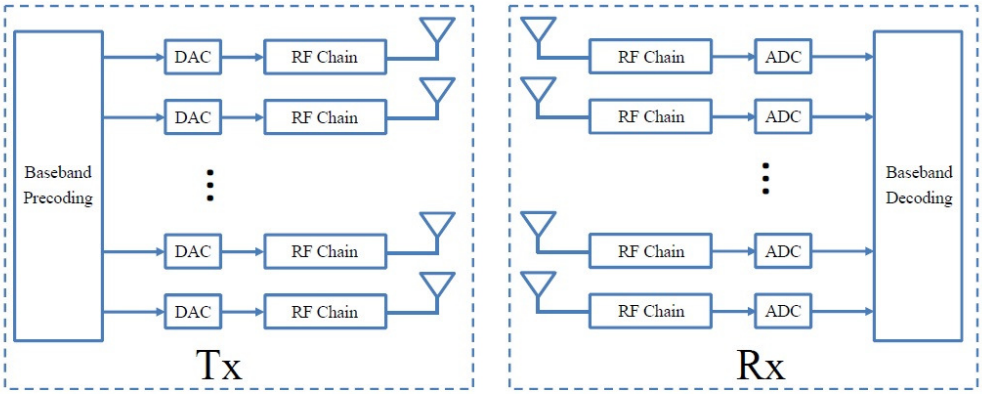

Figure 2.8. *Digital beamforming architecture*

There are also other beamforming techniques which are based on CSI of the channel. We will discuss later in the text.

There are three basic architectures for mmWave beamforming, including analog beamforming, hybrid beamforming and digital beamforming. In the next subsections it will be discussed why the analog beamforming is the more appropriate for mobile mmWave applications.

2.3.1 Digital beamforming

In digital beamforming each antenna is connected to its own RF chain and either a DAC or ADC as can been seen from figure 2.8. This makes the digital beamforming more flexible than analog and hybrid beamforming from the point of view of the signal processing [16].

Unfortunately, this technique present many disadvantages that do not allow to use it for mm-Wave applications. First of all, it is not possible to integrate an RF chain for every radiating element in a small area like the one dedicated to the arrays for mm-Wave. In fact, it is important to remember that a RF chain consists of a low-noise amplifier, a frequency down-convert, digital to analog converter (DAC), analog to digital converter (ADC) and so on [17]. Another problem, especially for mobile applications, would be the high power consumption. Finally, there could be Gigabits of data for each RF chain to process in a single second, and such high total data rate from all RF chains is a challenge for current baseband signal processing hardware [16].

2.3.2 Hybrid beamforming

Hybrid beamforming is unifying the characteristics of both analog and digital beamforming.This option has captured the attention of the scientists because it allows to reduce the hardware complexity that is characterizing the digital beamforming schemes, but at the same time is able to reach almost the same performance.

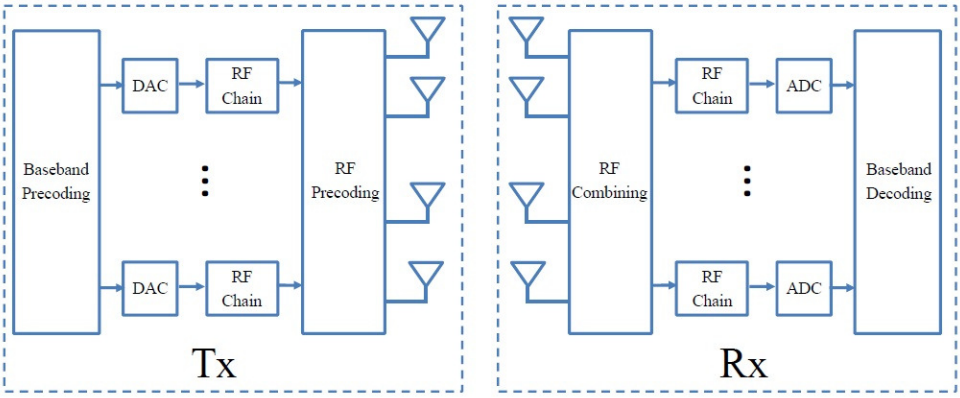

Figure 2.9. *Hybrid beamforming architecture*

The extra digital processing permits to have more degrees of freedom then the analog case but at the same time offers the opportunity to support multi-user transmission. As shown in 2.9, the hybrid beamforming has usually the same architecture of the digital beamforming but all the RF chain include a unique RF precoding block before passing the signals to the antennas.

Since in mmWave system there is a large available bandwidth which causes the presence of frequency selective fadings, in [18] it is proposed an hybrid beamformer model for broadband mmWave systems. In particular it is shown that the optimization in the broadband scenario can be achieved through the same procedure as in the narrowband scenario.

2.3.3 Analog beamforming

Analog beamforming is probably the easiest technique for developing MIMO in mmWave systems. Each antenna is connected to its own phase shifter and all the phase shifters are linked to a single RF chain, as can be seen from figure 2.10. It is possible to adjust the phase shifter weight via software, in order to satisfy the desired objective. The only limitation to the analog beamforming is represented by the fact that this technique is using quantized phase shifts and that is not possible to adjust the amplitude of the signals. This is the reason why it is more difficult to finely tune the beam and steer nulls [19]. Since it is the easiest to implement from the point of view of the hardware needed, this technique is the most used for mmWave communications.

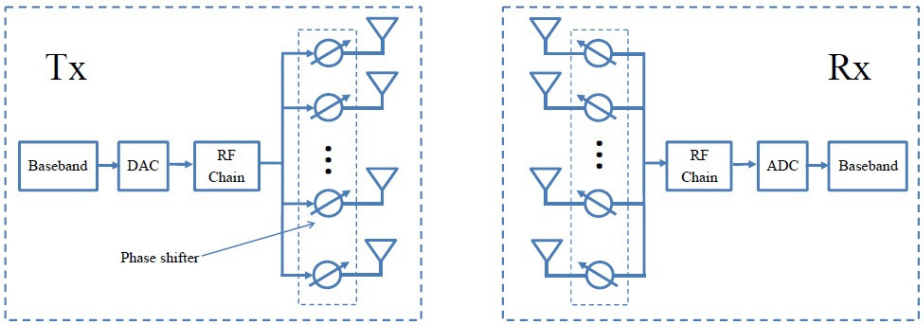

Figure 2.10. *Analog beamforming architecture*

2.4 Time delay vs phase

We want to consider the signal propagation in the case of a uniform array composed by N isotropic antennas as shown in 2.11. Assuming the array is in the far field when receiving the signal, the wavefront can be considered to be planar.

The propagation distance difference between the elements is:

$$d_e = d \sin \theta$$

Which creates a phase difference between two adjacent element of:

$$\Phi = 2\pi \frac{d \sin \theta}{\lambda}$$

So every signal will experience a propagation delay difference:

$$\tau = \frac{d_e}{c} = \frac{d \sin \theta}{c} = \frac{d \sin \theta}{f_c \lambda}$$

Thus, the delayed RF signal can be written as:

$$v_{bp}(t-\tau) = Re[v(t-\tau)e^{j\omega_c(t-\tau)}] = Re[v(t-\tau)e^{-j2\pi \frac{d \sin \theta}{\lambda}} e^{j\omega_c t}] = Re[v(t-\tau)e^{j\Phi} e^{j\omega_c t}] \tag{2.15}$$

where $\Phi = 2\pi d \frac{d \sin \theta}{\lambda}$.

As we can see the delay is affecting both the modulation and the carrier. If we consider that the modulation changes at a much slower ratio than the carrier it is possible to approximate $v(t-\tau)$ as $v(t)$.

This approximation is usually done when we are considering narrowband signals. It is important to notice that this is only an approximation because the signals are not actually shifted in the time domain. In fact the effect is to change only phase, in order to make it similar to the signal shifted in time. A signal is said to be narrowband if its bandwidth is narrow enough to conclude that the signals received at its extremity will combine in a

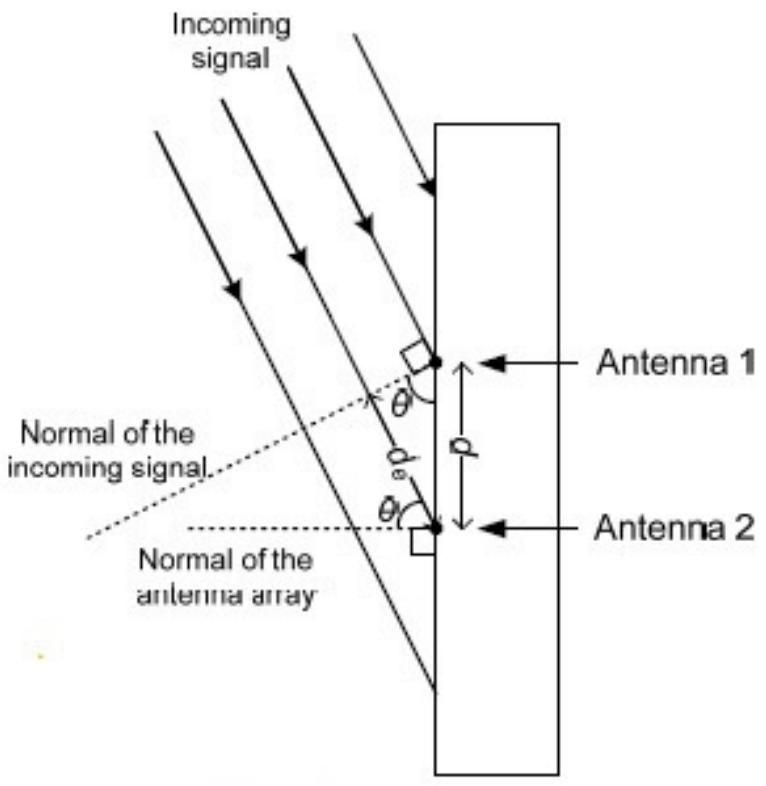

Figure 2.11. *Geometry of the received signal*

coherent way. In order to exploit the characteristics of the narrowband signals, in these cases it is usually more common to generate a phase shift instead of delaying the signal in the time domain. In this way,to apply the beamforming it will only be needed to apply the correct phase shift, weight the amplitudes of the signals and sum them in such a way that they will combine coherently.

3 MODELING OF BEAM SQUINT

In this chapter the beam squint models for different array geometries are derived. It is studied how the different array geometries are affected by this problem depending on different parameters by simulating their responses with the software Matlab.

From the analysis of the previous paragraph, it is important to notice the delay τ in equation 2.15 is not always negligible and it is particularly important in mm-wave communications, where very wide bandwidths are used. In general, every antenna of the array will receive a copy of the transmitted signal $v(t)$ characterized by a certain delay. All the received signals can be collected in a vector:

$$\mathbf{v}(\mathbf{t},\theta) = \left[v(t), ..., v\left(t - \frac{(n-1)d\sin\theta}{c}\right), ..., v\left(t - \frac{(N-1)d\sin\theta}{c}\right)\right]^T \tag{3.1}$$

which can be rewritten as follows by applying the Fourier transform:

$$\mathbf{V}(\mathbf{f},\theta) = V(f)\left[1, e^{j2\pi c^{(-1)} fd\sin\theta}, ..., e^{j2\pi c^{(-1)} f(n-1)d\sin\theta}, ..., e^{j2\pi c^{(-1)} f(N-1)d\sin\theta}\right]^T \tag{3.2}$$

Therefore, it is possible to express the received signal $y(t)$ as the sum off all the delayed component of the original signal $v(t)$ present in 3.1 and will result in:

$$\mathbf{Y}(\mathbf{f},\theta) = \sum_{n=1}^{N} V(f) e^{j2\pi c^{(-1)} f(n-1)d\sin\theta} \tag{3.3}$$

We can notice that the gain provided by a phased array is is depending on the frequency in the wideband system due to the time delays that cannot be approximated anymore. This effect is the so-called beam squint phenomenon.

The beam squint phenomenon is caused by approximating time delays with simple phase shifts in an analog beamformer. It is extremely important to notice that not only the array response will depend on the frequency, but it will also depend on the angle that has been considered. Thus, frequency and angular responses of the array are two different faces of the same coin and they will always present symmetric characteristics.

The effects generated by the beam squint phenomenon are directly proportional to differ-

ent characteristics of the array:

1. The AoA θ
2. The number of radiating elements N
3. The bandwidth of the signal B

Figure 3.1 presents an example on how the parameters listed above are influencing the array response in the angular domain. In general, it is possible to conclude that increasing each parameter will introduce an shift of the maximum gain of the subcarrier. Moreover, if we consider a subcarrier different from the center one, we will noticed that the transmission will also experience a gain loss towards the desired direction. As can be noticed from figure 3.1(c), the changes to which the pattern is subjected in the frequency domain can also be considered to be symmetrical to the variations that could be obtained for a fixed AoA but for different subcarriers [16]. In particular, subcarriers with center frequency lower than the carrier will present the maximum gain shifted towards higher angles, while subcarriers with center frequency higher than f_c will have their maxima shifted towards lower angles. In general, the effects of beam squint increase as the angle diverges from the beam focus angle, but it also tends to become higher when the beam focus angle increases.

The effects of the frequency selectivity introduced by the wideband system are shown in figures 3.2 and 3.3. It is immediate to notice that the frequency response is highly affected by the beam squint problem. In fact, as can be seen from the figures, arrays containing a not elevated number of elements are characterized by a more constant gain in all the subcarriers. Instead, the higher is the number of elements in the array, the bigger is the gain loss experienced at the edges of the band compared to the center frequency. Moreover, figure 3.3 shows that the effects are more visible when a larger bandwidth is available if compared to the case of figure 3.2.

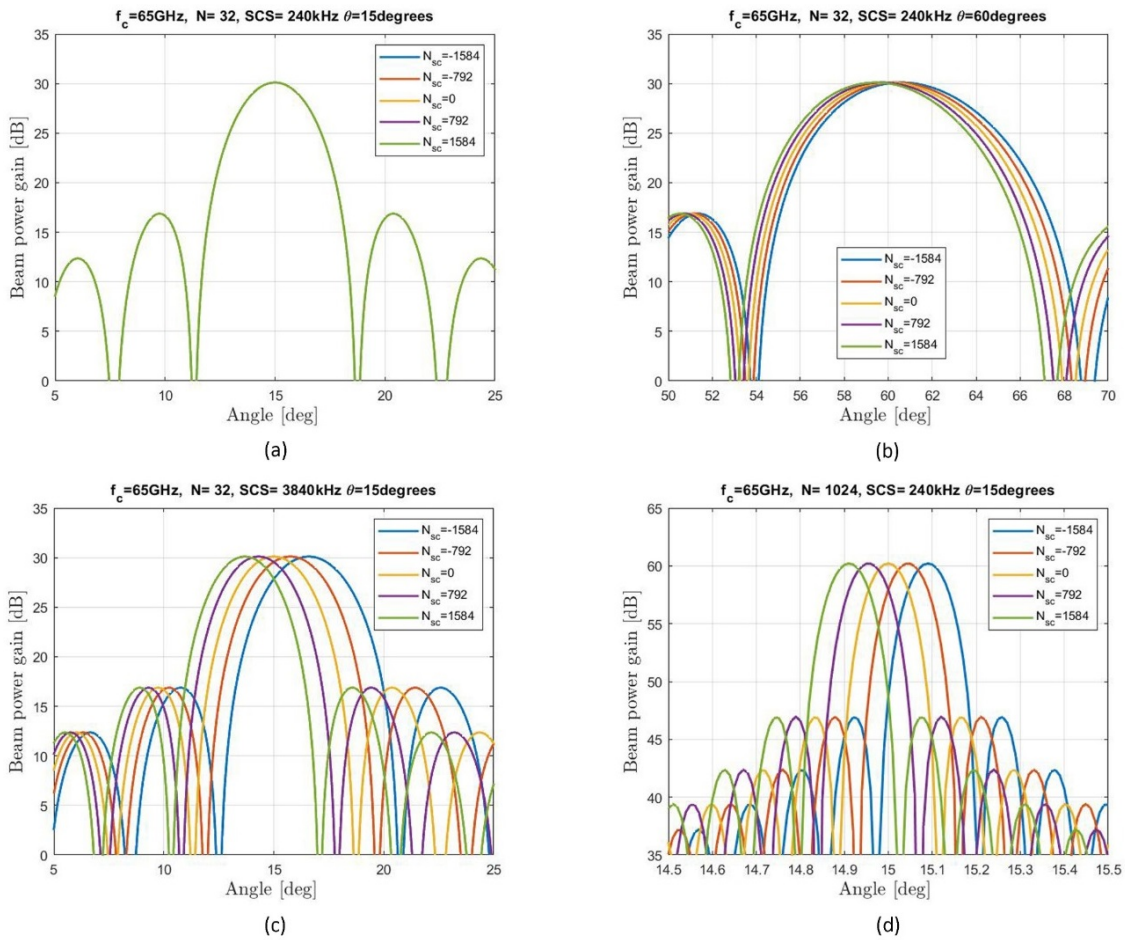

Figure 3.1. *Beam squint effects: a)Ideal case without beam squint b) Beam squint effect when the AoA is increased c) Beam squint effect when the CBW is increased d)Beam squint effect when the number of elements in the array is increased*

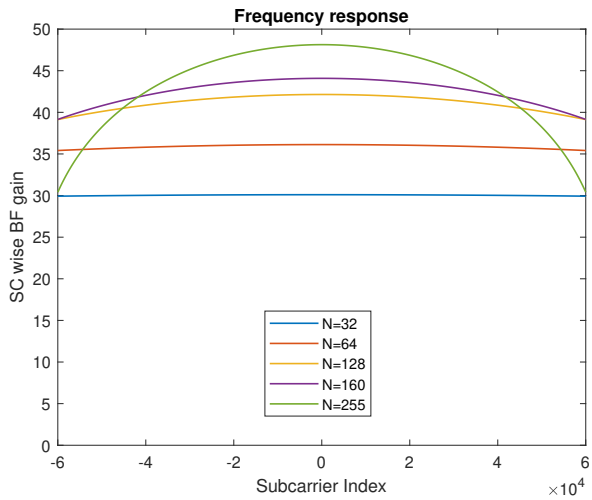

Figure 3.2. *Frequency response of an array with carrier frequency at 65GHz, Target direction of 30° and CBW=1.8GHz*

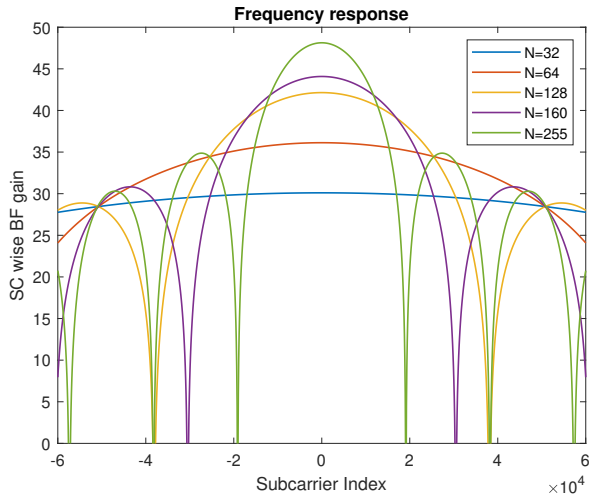

Figure 3.3. *Frequency response of an array with carrier frequency at 65GHz, Target direction of 30° and CBW=6.4GHz*

In the frequency range from $57GHz$ to $71GHz$, very wide CBWs are possible when operating in unlicensed and licensed band. Due to the very high CBW to carrier frequency ratio that can be encountered when operating at these frequencies, and also due to the very large antenna arrays required to overcome the increased pathloss and atmospheric attenuation, beam squint problem may be significant and cannot be neglected. Thus, it needs to be taken into consideration in the system design.

It is important to notice that the beam squint has not always been seen as a negative phenomenon. In fact, it was used is the firsts phased array in order to modify the beam in what are called frequency-scan arrays [20].

3.1 ULA

When considering a receiving linear array composed of N isotropic antennas and with an element distance d, based on figure 2.11, it is possible to write the sum of all the received signals as:

$$x(t) = \sum_{n=1}^{N} w_n e^{-j(n-1)\Phi} v(t-(n-1)\tau) \tag{3.4}$$

where $\Phi = 2\pi \frac{d \sin\theta}{\lambda}$.

We can refer to the elements $e^{-j(n-1)\Phi}$ as a vector $S(\Phi)$. The coefficient w_n are usually chosen to be the complex conjugate of the $S(\Phi)$ for a desired AoA. Thus $w_n = S(\Phi_d)^*$ where $\Phi_d = 2\pi \frac{d \sin\theta_d}{\lambda}$.

We can rewrite the received signal as:

$$x(t) = \sum_{n=1}^{N} e^{j(n-1)\Phi_d} e^{-j(n-1)\Phi} v(t-(n-1)\tau) = \sum_{n=1}^{N} e^{j(n-1)(\Phi_d-\Phi)} v(t-(n-1)\tau) \tag{3.5}$$

If we apply the Fourier transform we can derive this expression:

$$X(f) = \sum_{n=1}^{N} e^{j(n-1)(\Phi_d-\Phi)} e^{-j2\pi f(n-1)\tau} V(f) \tag{3.6}$$

We are interested in simulating the behaviour of the coefficients that are multiplying V(f). V(f) is depending on the angle of arrival θ, frequency, number of elements N and element distance d. To better understand the dependency of this equation from the parameters we can rewrite it as:

$$R(f) = \sum_{n=1}^{N} e^{j(n-1)(\Phi_d-\Phi)} e^{-j2\pi f(n-1)\tau} = \sum_{n=1}^{N} e^{j\frac{2\pi d}{\lambda}(n-1)(\sin\Phi_d - \sin\Phi)} e^{-j2\pi f(n-1)\frac{d\sin\theta}{c}} \tag{3.7}$$

All the simulations were made considering a signal with carrier frequency of $f_c = 65GHz$. It is extremely important to underline that the variable f of the previous expression refers to the baseband signal. It is also important to notice that in order to compare the achieved result, the gain pattern is always plotted both for the nominal and the averaged configurations.

The averaged plot is obtained by plotting the function for every desired angle of arrival in the frequency domain, integrating it over the variable f for obtaining a vector which gives

Table 3.1. *Table of the variations depending on different number of elements for ULA*

$Number\ of\ elements\ (N)$	$Gain\ Loss\ (dB)$	AoA	$HPBW$
$N = 36$	0.6	14.96°	3.28
$N = 256$	7.18	14.26°	2.38
$N = 1024$	13.0	14.19°	2.38

us the power for every desired θ_d and plotting $P_x(\theta)$ as a function of θ.

The integration over the frequency domain was done by summing the square of the absolute value of each frequency component.

3.1.1 Different number of elements

Given the expression 3.7 it was first studied how a change in the number of elements is influencing the total pattern. All the simulations were done using an element spacing of $d = \lambda/2$, choosing the desired angle of arrival to be $\theta_d = 15°$ and by using a channel bandwidth of 10GHz.
Intuitively, it is immediate to think that an higher number of elements will results in a bigger delay between the first and the last elements of the array. These simulations were done for arrays of 36, 256 and 1024 elements. The results are respectively shown in figure 3.4 and 3.5. Comparing the two figures it is immediate to notice that when more antennas are used in the array the nominal lobe is becoming narrower around the desired AoA, but at the same time the beam squint effect is becoming more significant. This is due to the fact that the first and last element of the array will experience a much higher delay between them.

From the figures, it is evident that the beam quint phenomenon is causing a spreading of the main lobe on the angular domain and a very significant loss in the maximum gain achieved by the array. This is more evident when arrays with big sizes are taken into consideration, like in figure 3.5, where it is demonstrated that the average case presents a gain loss of $13dB$.

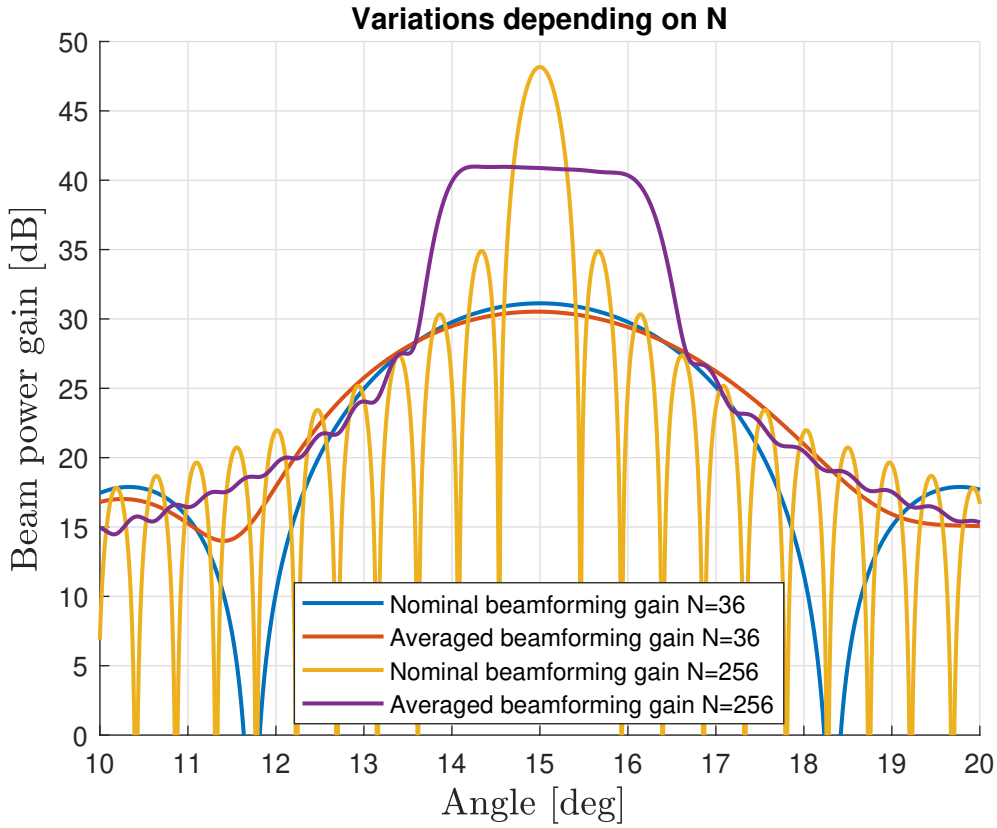

Figure 3.4. *Nominal and averaged plot for arrays with 36 and 256.*

3.1.2 Variations depending on AoA

Finally, it was studied how different desired AoA will influence the main lobe. It is intuitive to think that for bigger angles the effect due to the beam squint phenomenon will produce more aggressive changes. This was also confirmed by the simulations. In fact, it was demonstrated that for a desired angle of arrival of 0°the nominal and average configuration match exactly as can be seen from 3.6. On the other hand, when the desired angle of arrival is increasing it is possible to notice from figure 3.6 that the main lobe is getting wider and reaches a lower power value because of the frequency dispersion.

This is something that we should absolutely take into account because it is important especially for the downlink communications. In fact, we know that every base station is serving a particular cell. Each cell can be subdivided in sectors to achieve better performance. Now it is important to understand that, depending on the number of sectors, the AoA can assume different maximum values. Here we considered a maximum angle of arrival of 60°, which implies that the cell is divided in 3 sectors each of 120°.

In order to have a quantitative analysis of the achieved results for ULA arrays, the numerical variations between average and nominal configurations were collected in 3.2. To have a numerical comparison between all the cases, we focused on studying the difference between the maximum gain obtained in the ideal case with the averaged maximum, the shift of the desired AoA and the $3dB$ bandwidth dispersion.

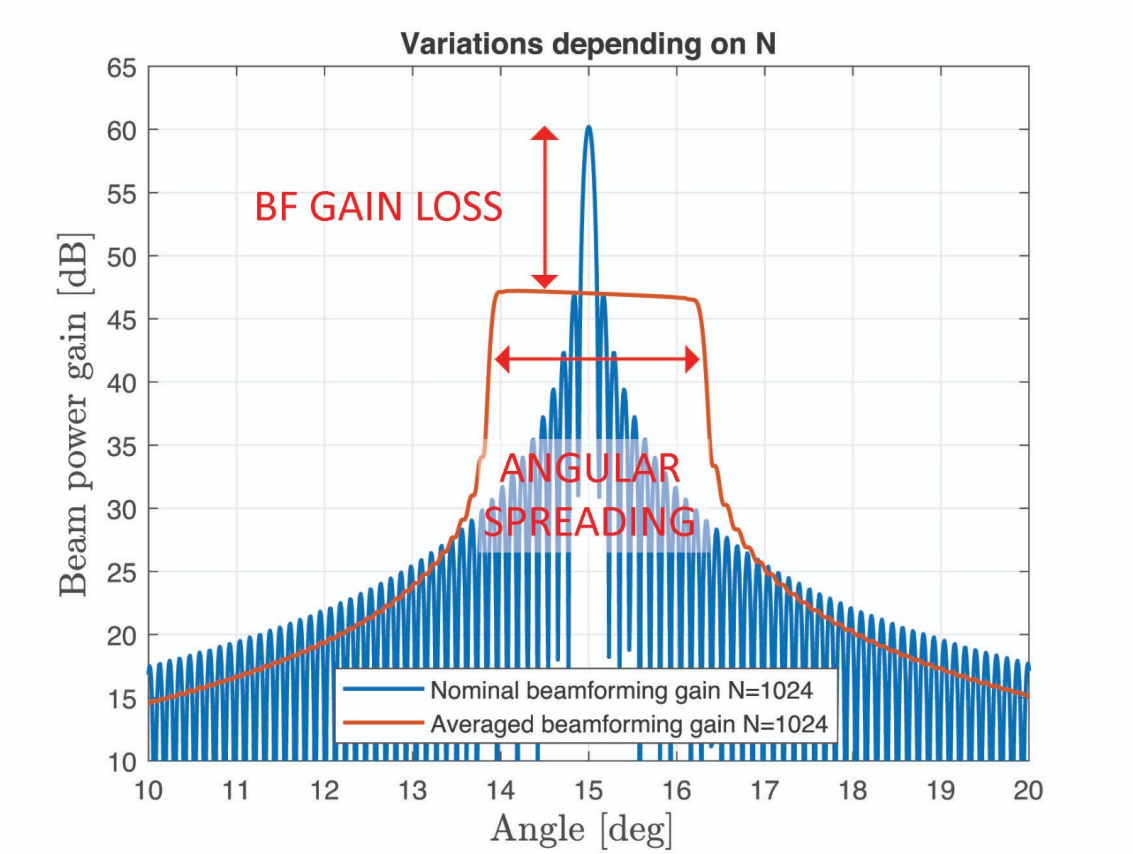

Figure 3.5. *Nominal and averaged plot for array with 1024 elements.*

Table 3.2. *Table of the variations depending on different desired* AoA

$Desired\ AoA$	$Gain\ Loss\ (dB)$	$Variation\ AoA$	$HPBW$
$\theta_d = 0°$	0	0°	0.08
$\theta_d = 15°$	12.99	0.81°	2.38
$\theta_d = 30°$	15.80	1.92°	5.16
$\theta_d = 60°$	18.15	5.69°	16.37

3.1.3 Variations depending on CBW

Finally, it was interesting to study how the channel bandwidth is influencing the effects created by the beam squint problem. As mentioned in the previous chapter, the beam squint is due to a frequency dependency of the received signal. Thus, we are expecting to face a bigger effect when using a larger channel bandwidth. This is due to the fact that the element spacing is usually equal to half wavelength of the carrier frequency $d = \lambda_c/2$, but every subcarrier in the channel will have a center frequency which is different from it. The larger is the bandwidth, the larger will be the difference between the expected

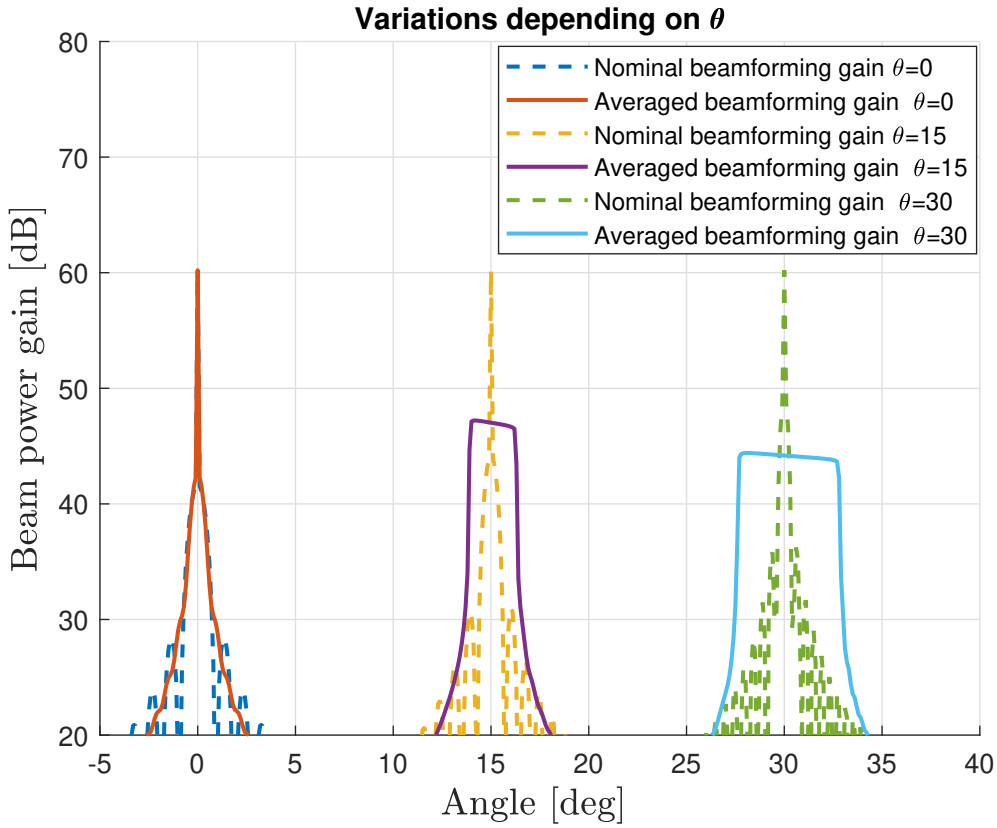

Figure 3.6. *Nominal and averaged plot for arrays with different* AoA

element distance and the real one, this is why the effect of the beam squint will be higher.

Figures 3.7 and 3.8 show the beam squint phenomenon on the angular domain for two arrays including respectively 36 and 256 elements for different CBW and AoA of 30°. It is immediate to notice that the beam squint causes BF gain loss and angular spreading that are increasing both with CBW and with the number of elements.

To have a better understanding of the variations introduced, the gain loss and the angular spread towards desired direction for different combinations of channel bandwidths and size of arrays are shown in the tables 3.3 and 3.4.

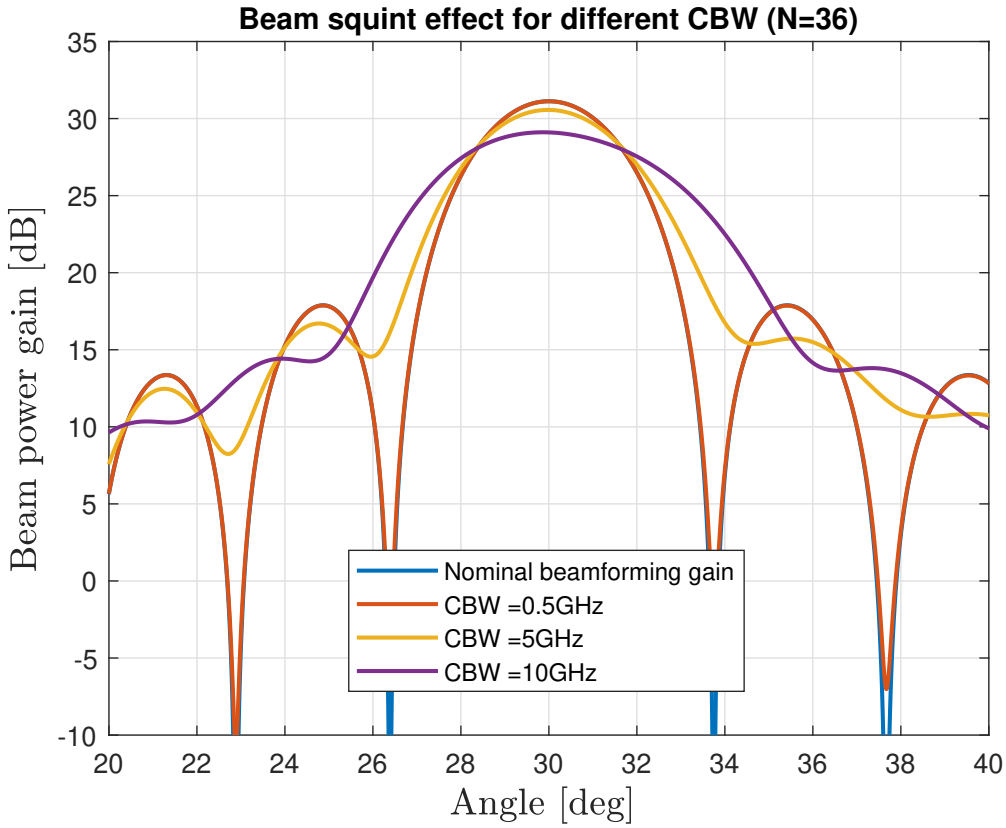

Figure 3.7. *Beam squint phenomenon for an array of 36 elements with different CBW*

Table 3.3. *Table of the beamforming gain loss with respect to ideal beamforming [dB]*

CBW (GHz)	0.4	0.8	1.6	3.2	6.4	10.0
$N = 36$	0.0044	0.0175	0.0697	0.2755	1.0503	2.2990
$N = 128$	0.0551	0.2186	0.8428	2.8168	5.5843	7.3722
$N = 256$	0.2186	0.8428	2.8183	5.6137	8.4441	10.2494
$N = 1024$	2.8188	5.6152	8.5063	11.427	14.3195	16.1392

3.2 UPA

In the previous paragraph we examined the case of the linear array including the beam squint. Now it is interesting to extend this concept also to the case of a uniform planar array (UPA).

The geometry used in this case is shown in 3.9. It consist of a planar array of dimensions MxN, where the lower-left antenna is assumed to be in the position (1,1,0) and the generic element can be referred to as (p,q,0).

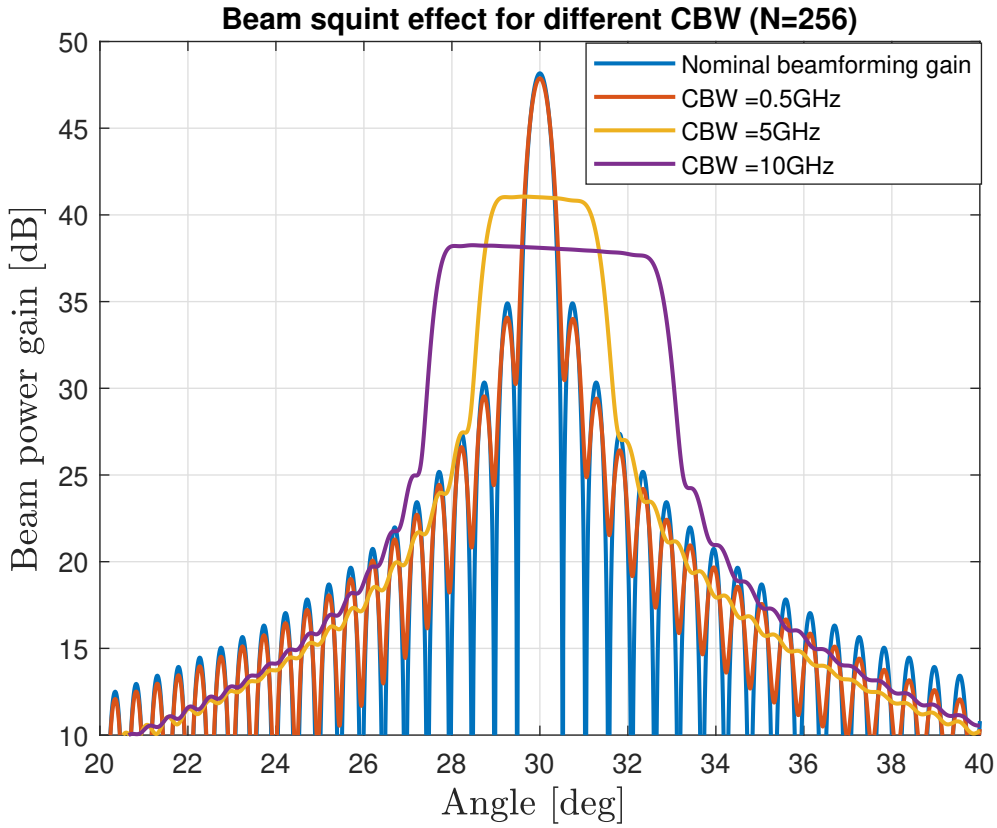

Figure 3.8. *Beam squint phenomenon for an array of 256 elements with different CBW*

Table 3.4. *Table of the angular spread towards desired direction*

CBW (GHz)	0.4	0.8	1.6	3.2	6.4	10.0
$N = 36$	3.00	3.00	3.03	3.15	3.76	5.28
$N = 128$	0.84	0.87	1.00	1.67	3.31	5.16
$N = 256$	0.43	0.50	0.83	1.64	3.29	5.15
$N = 1024$	0.20	0.40	0.81	1.64	3.29	5.16

We are interested in observing the signal coming from the point P which is assumed very far compared to the dimensions of the array. If we consider two different antenna elements of the array, one in positions $(1, 1, 0)$ and the other in $(p, q, 0)$, it is possible to see from the picture that the two antennas will experience a different delay of the receiving signal because it has to travel the distances d_{11} and d_{pq} for reaching the respective antennas.

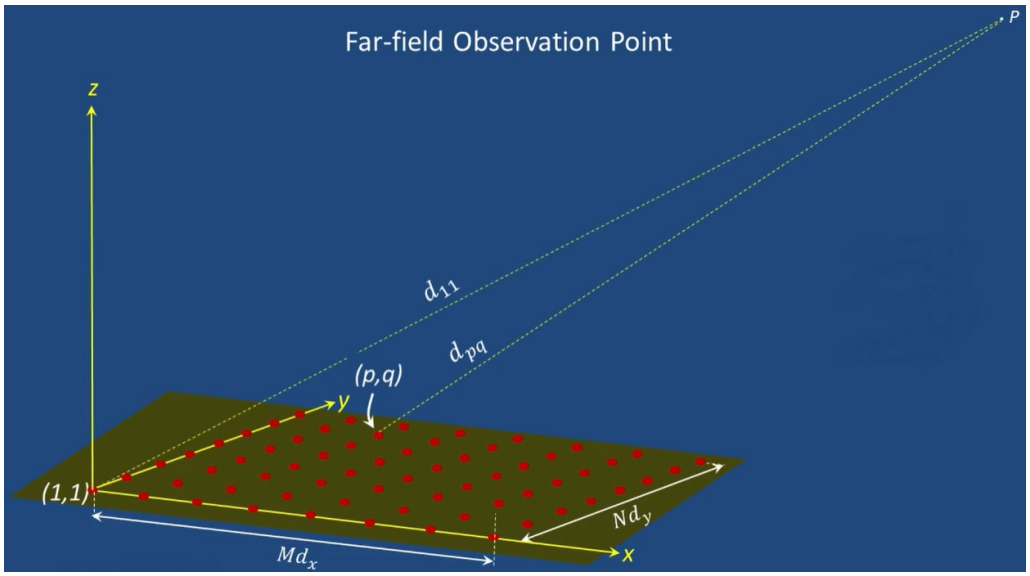

Figure 3.9. *Cartesian geometry*

Thus, the delay experienced by the different elements can be calculated as:

$$\tau = \frac{d}{c} = \frac{d_{11} - d_{pq}}{c} \tag{3.8}$$

If we consider $\vec{r}$ to be the vector from (1,1) to P it can be expressed as:

$$\vec{r} = r_x \hat{u_x} + r_y \hat{u_y} + r_z \hat{u_z}.$$

Since we are using a 3-dimensional space it could be useful to introduce a spherical coordinate system. In the following it is used the coordinate systems shown in 3.10.

In this new coordinate system, the component of $\vec{r}$ can be expressed as:

$$\begin{aligned} r_x &= \sin\theta\cos\phi \\ r_y &= \sin\theta\sin\phi \\ r_z &= \cos\theta \end{aligned} \tag{3.9}$$

In the same way, the vector $\vec{r_{pq}}$, which is departing from (1,1,0) and which points to $(p, q, 0)$ can be expressed as:

$$\vec{r_{pq}} = (p-1)d_x\hat{u_x} + (q-1)d_y\hat{u_y}$$

We are interested in computing the projection of $\vec{r_{pq}}$ on the line whose unit vector is $\vec{r}$, because it is the length difference between the distance that a wave generated in P will

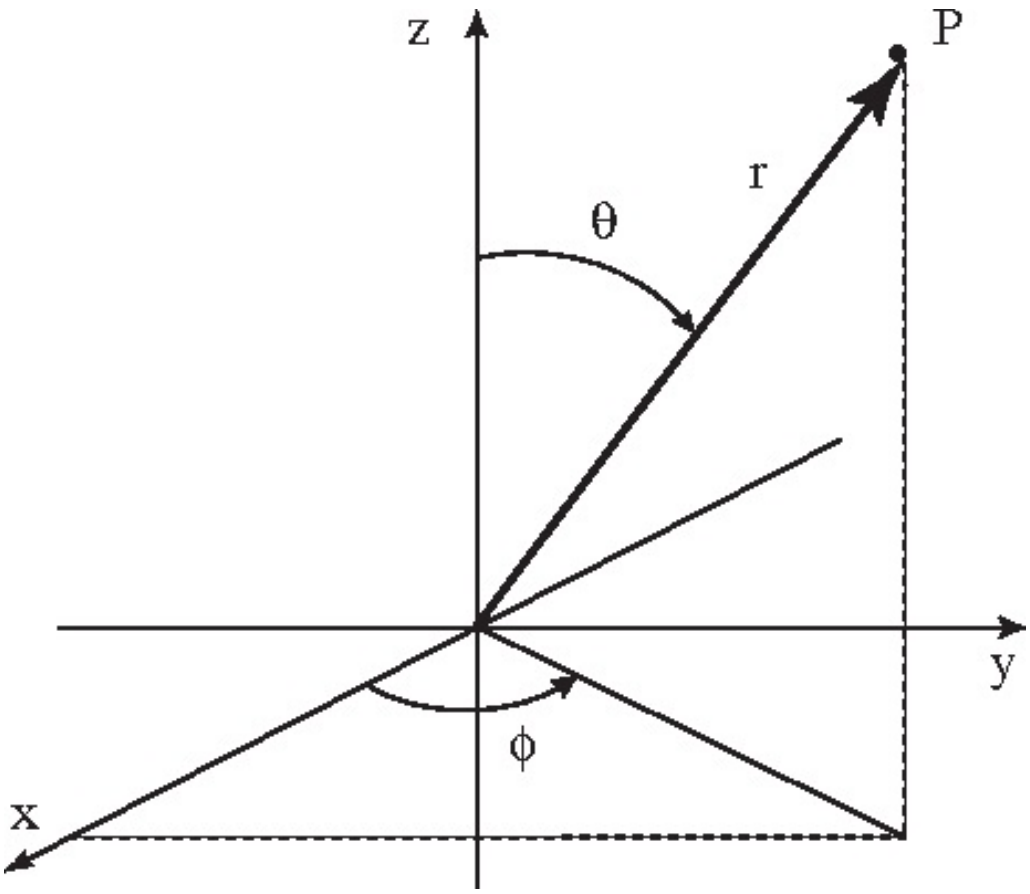

Figure 3.10. *Polar coordinate system*

have to travel for reaching $(1, 1, 0)$ after being arrived in $(p, q, 0)$. We call this length path difference Δl_{pq}.

The path difference can be calculated as the scalar multiplication of the vectors $\vec{r}$ and $\vec{r_{pq}}$. Remembering that the scalar multiplication corresponds to summing the respective components we obtain:

$$\Delta l_{pq} = \vec{r} \cdot \vec{r_{pq}} = r_x(p-1)d_x\hat{u_x} + r_y(q-1)d_y\hat{u_y} \tag{3.10}$$

By substituting the polar expression of r_x and r_y we obtain:

$$\Delta l_{pq} = (p-1)d_x \sin\theta\cos\phi + (q-1)d_y \sin\theta\sin\phi \tag{3.11}$$

The signal received in P from (1,1,0) is:

$$s_{11}(t) = m(t)\cos(\omega_c t)$$

where $m(t)$ is the modulation factor and $\cos(\omega_c t)$ is the carrier.

The signal received from (p,q,0), instead, will arrived in advance. Thus it is possible to write:

$$s_{pq}(t) = s_{11}(t + \tau_{pq})$$

Following the same procedure described in section 3.1.3, we can write:

$$\begin{aligned} v_{bpq}(t+\tau_{pq}) &= Re[v(t+\tau_{pq})e^{j\omega_c(t+\tau_{pq})}] = Re[v(t+\tau_{pq})e^{j\omega_c t}e^{j\omega_c \tau_{pq}}] = \\ &= Re[v(t+\tau_{pq})e^{j\omega_c t}e^{j\omega_c \frac{\Delta l_{pq}}{c}}] = \\ &Re[v(t+\tau_{pq})e^{j\omega_c t}e^{j2\pi\frac{\Delta l_{pq}}{\lambda}}] \end{aligned} \tag{3.12}$$

we can call the term $2\pi\frac{\Delta l_{pq}}{\lambda} = \Phi_{pq}$. In the reception case, the total signal received can be written as:

$$x(t) = \sum_{p=1}^{M}\sum_{q=1}^{N} w_n v(t+\tau_{pq})e^{j\Phi_{pq}} \tag{3.13}$$

When moving to the Fourier domain we obtain:

$$X(f) = \sum_{p=1}^{M}\sum_{q=1}^{N} w_n e^{j\Phi_{pq}} e^{j2\pi f \tau_{pq}} V(f) \tag{3.14}$$

The coefficient w_n are usually chosen to be $w_n = S(\Phi_d)^*$. Thus we can rewrite the two first terms in the sum above as:

$$\begin{aligned} w_n e^{j\Phi_{pq}} &= e^{-j\Phi_{pq_d}} e^{j\Phi_{pq}} = e^{-j2\pi\frac{\Delta l_{pq_d}}{\lambda}} e^{j2\pi\frac{\Delta l_{pq}}{\lambda}} = \\ &= e^{-j2\pi/\lambda[(p-1)dx(\sin\theta\cos\phi - \sin\theta_d\cos\phi_d)] + (q-1)dy(\sin\theta\sin\phi - \sin\theta_d\sin\phi_d)} \end{aligned} \tag{3.15}$$

If we define:

$$u = \sin\theta\cos\phi \qquad u_d = \sin\theta_d\cos\phi_d \tag{3.16}$$

$$v = \sin\theta\sin\phi \qquad v_d = \sin\theta_d\sin\phi_d \tag{3.17}$$

we can introduce the quantities:

$$\Psi_x = \frac{2\pi}{\lambda} dx(u - u_d) \qquad \Psi_y = \frac{2\pi}{\lambda} dy(v - v_d) \tag{3.18}$$

and we can rewrite the coefficients of $V(f)$ in 3.14 as:

$$R(f) = \sum_{p=1}^{M} e^{j(p-1)\psi_x} \sum_{q=1}^{N} e^{j(q-1)\psi_y} \sum_{p=1}^{M} \sum_{q=1}^{N} e^{j2\pi f \tau_{pq}} \tag{3.19}$$

The coefficients $e^{j2\pi f \tau_{pq}}$ depend on the value of $f, p, q, d_x, d_y, \theta$ and ϕ as can be deduced from 3.11.
They can be written in a more compact way:

$$\begin{aligned} \sum_{p=1}^{M} \sum_{q=1}^{N} e^{j2\pi f \tau_{pq}} &= \sum_{p=1}^{M} \sum_{q=1}^{N} e^{j2\pi \frac{f}{c}[(p-1)d_x \sin\theta \cos\phi + (q-1)d_y \sin\theta \sin\phi]} = \\ &= \sum_{p=1}^{M} e^{j2\pi \frac{f}{c}(p-1)d_x \sin\theta \cos\phi} \sum_{q=1}^{N} e^{j2\pi \frac{f}{c}(q-1)d_y \sin\theta \sin\phi} \end{aligned} \tag{3.20}$$

Thus, we can introduce two new quantities:

$$G_x = \frac{2\pi u}{\lambda} d_x u \qquad G_y = \frac{2\pi v}{\lambda} d_y v \tag{3.21}$$

So the coefficients that we are interested in plotting can be written as:

$$\sum_{p=1}^{M} e^{j(p-1)G_x \frac{f}{f_c}} \sum_{q=1}^{N} e^{j(p-1)G_y \frac{f}{f_c}} \tag{3.22}$$

Finally, the total expression of the received signal in the frequency domain can be written as:

$$R(f) = \sum_{p=1}^{M} e^{j(p-1)(\psi_x + \frac{f}{f_c} G_x)} \sum_{q=1}^{N} e^{j(q-1)(\psi_y + \frac{f}{f_c} G_y)} \tag{3.23}$$

3.2.1 Different number of elements

Also for the planar case it is interesting to study how the different parameters are influencing the angular and frequency responses of the arrays.

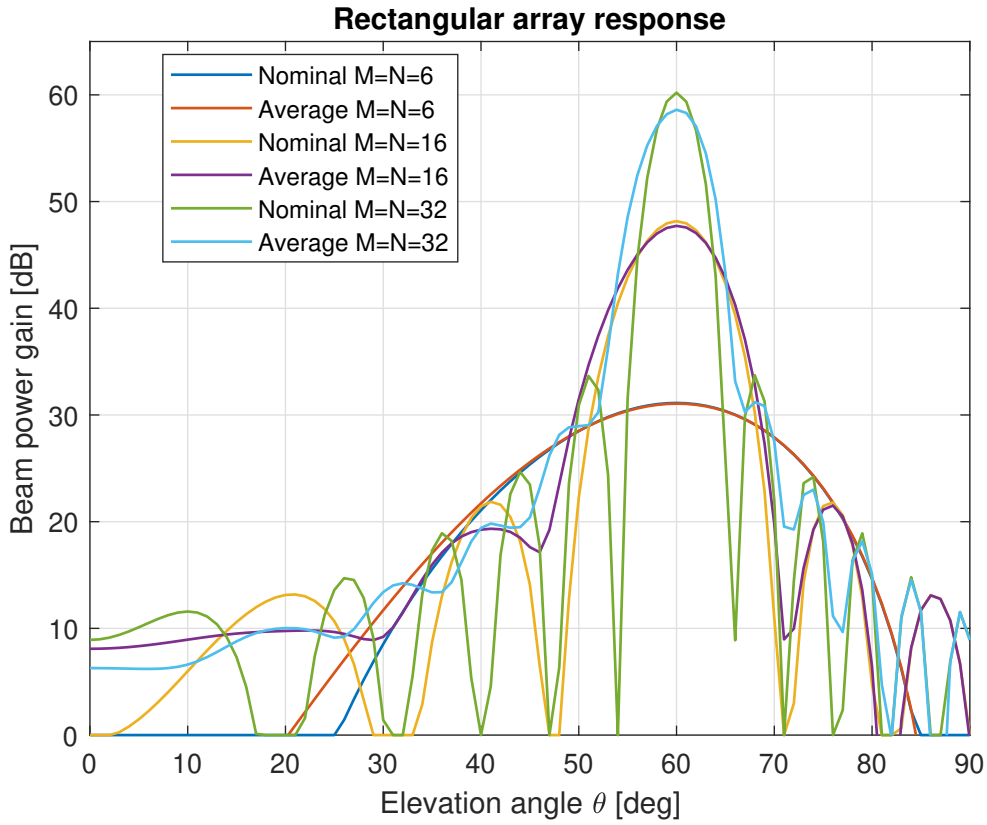

Figure 3.11. *Rectangular array response for UPA arrays with different number of elements*

In this section the effects of varying the number of elements in the array are studied. In order to have results that are comparable with the ones of the ULA case, the geometries studied present the same total number of elements as the ones studied in section 3.1.3. Thus, were used arrays with dimensions respectively of $6x6$, $16x16$ and $32x32$. All the simulations were carried out considering a carrier frequency $f_c = 65GHz$ with a channel bandwidth of $10GHz$. In these simulations the AoA was identified by the pair $(\theta_d, \phi_d) = (60°, 45°)$. All the results in this and the following subsections are expressed in the Matlab coordinate system, where the elevation angle is growing from the xy-plane towards the positive z-axis.

It was of particular interest to notice that the results are not influenced by the choice of ϕ_d, instead they depend only on the elevation angle as will be shown in the next section.

Figure 3.11 represents the results of the simulation on the azimuth cut for the desired phi_d. It is evident that the lower is the number of the elements in the array, the lower is also the beam squint effect. In fact, for array size of 6x6 the nominal and average plots are coinciding.

On the other hand, an increase in the array size implies that the $HPBW$ gets wider and the average main lobe presents a lower gain compared to the nominal.

The results showing how the gain loss and $HPBW$ are changing with respect to the

number of elements are collected in table 3.5.

Comparing the results of tables 3.1 and 3.5 is immediate to notice how the gain loss in the planar array case is extremely reduced. In particular, as can be seen from 3.11, a planar array with 1024 elements will present a maximum gain of $58.61dB$ considering the frequency dependency, while in the linear case the maximum achievable gain was $47dB$.

It is also possible to notice that, as expected, the main lobe is becoming narrower as the number of elements is increasing, but the $HPBW$ for the average cases are showing a bigger angular spread compared when the increasing the number of elements.

Moreover, it is important to underline that the performances of the array are strictly related with the desired elevation angle. For example, it was noticed that the beam squint effect is more persistent when considering elevation angles that closer to the xy-plane. On the other hand, if the desired direction of arrival is coinciding with the z-axis it is possible to notice that there is no difference between the average and nominal case.

3.2.2 Variations depending on AoA

The angle of arrival is a crucial parameter for the beam squint phenomenon. Since we are considering an uniform planar array, the AoA will be characterized by a pair (el, az).

As was mentioned in the previous subsection, the first thing that was noticed is that the azimuth angle ϕ_d is not influencing at all the performances of the array. This is something unexpected if looking at the geometry of the array. In fact, since a rectangular array is not symmetric from its center, we would expect that for angles like $\phi_d = 45°$ the response would change significantly, because the signal is impinging on the corner of array. On the other hand, the elevation angle of arrival is assuming a particular role in the behaviour of the array response. In fact, the more the θ_d is getting close to the xy-plane, the higher will be the effect of the beam squint. This is also confirmed by the results in table 3.6 and figure 3.12. In this subsection all the simulations were done considering an array of dimensions $MxN = 1024$, with a channel bandwidth of $10GHz$.

The results in table 3.6 are confirming what was stated before. In fact, for low elevation

Table 3.5. *Table of gain loss and HPBW variation depending on different number of elements for an UPA array*

$Number\ of\ elements$	$Gain\ Loss\ (dB)$	$HPBW\ av$	$HPBW\ nom$
$MxN = 36$	0.06	21 °	21°
$MxN = 256$	0.44	10°	8°
$MxN = 1024$	1.60	6°	4°

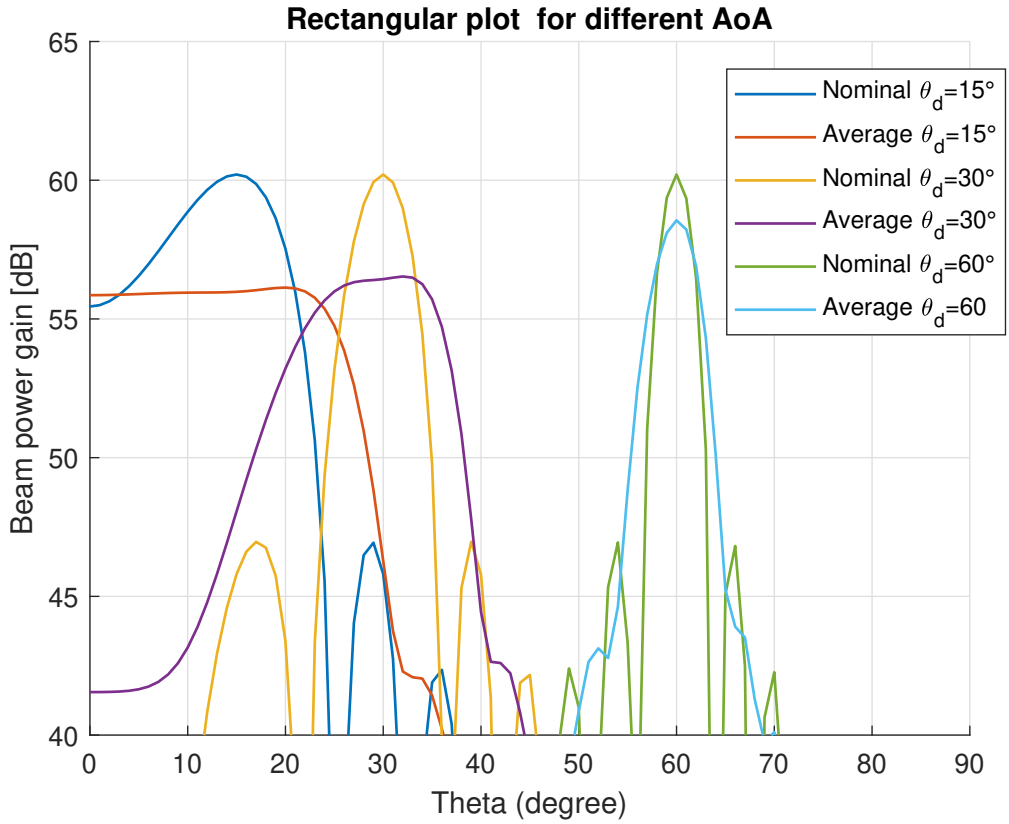

Figure 3.12. *Rectangular array response for UPA arrays with receiving signals from different elevation angles*

angles, which in Matlab coordinate system are very close to the xy-plane, the gain loss is higher than for angle which are getting closer to the z-axis.

Considering the HPBW, instead, is extremely important to notice it is decreasing while the elevation angle increases. A particular results is obtained in the case of very low elevation angle: in these cases, in fact, the average beamforming gain gets much wider compared to the nominal. This characteristic can potentially lead to the usability of the array in these directions.

Table 3.6. *Table of gain loss and HPBW variation depending on different number of elements for an UPA array*

$AoA\ (el)$	$Gain\ Loss\ (dB)$	$HPBW\ av$	$HPBW\ nom$
$15°$	4.08	54°	15°
$30°$	3.68	17°	8°
$60°$	1.65	6°	4°

3.2.3 Variations depending on CBW

The last simulations for the UPA array were the ones regarding the effects caused by the changes of the channel bandwidth. As in the case of the linear array we would expect that an increase of the channel bandwidth would imply a more strong presence of the beam squint phenomenon. For very wide channels, in fact, we are expecting an extremely high gain loss and a very high dispersion both on the frequency and angular responses. In this subsection the simulations were made considering an array of size $MxN = 32x32$ and an angle of arrival AoA identified by the pair $(\theta_d, \phi_d) = (60°, 45°)$.

The results of table 3.7 confirm the benefit of utilizing a planar array instead of a linear one. In fact, even with extremely wide channel bandwidth the gain loss is reduced consistently and the angular dispersion obtained for planar arrays is not so relevant if compared to the respective channel bandwidth. This is the reason why table 3.7 is reporting only the results obtained by varying the CBW of very large steps. The results show that an angular dispersion of only 2°is present with a channel bandwidth of 10GHz while, as shown in 3.4, for a linear array it was approximately 5°. This is a very good improvement when considering the performance of the array. The main benefits of the planar array are not only seen in the improved CBW, but mainly in the higher gains obtained. A linear array with 1024 elements and $CBW = 10GHz$ is presenting a gain loss of $16dB$, instead a planar array with the same number of elements has a loss of only $4dB$ which means that the gain was improved of almost the 20% compared to the linear case.

Table 3.7. *Table of gain loss and HPBW variation depending on the channel bandwidth for an UPA array*

$CBW\ (GHz)$	$Gain\ Loss\ (dB)$	$HPBW\ av$	$HPBW\ nom$
$0.5GHz$	0.005	4°	4°
$5GHz$	0.44	4°	4°
$10GHz$	1.60	6°	4°
$20GHz$	4.08	11°	4°

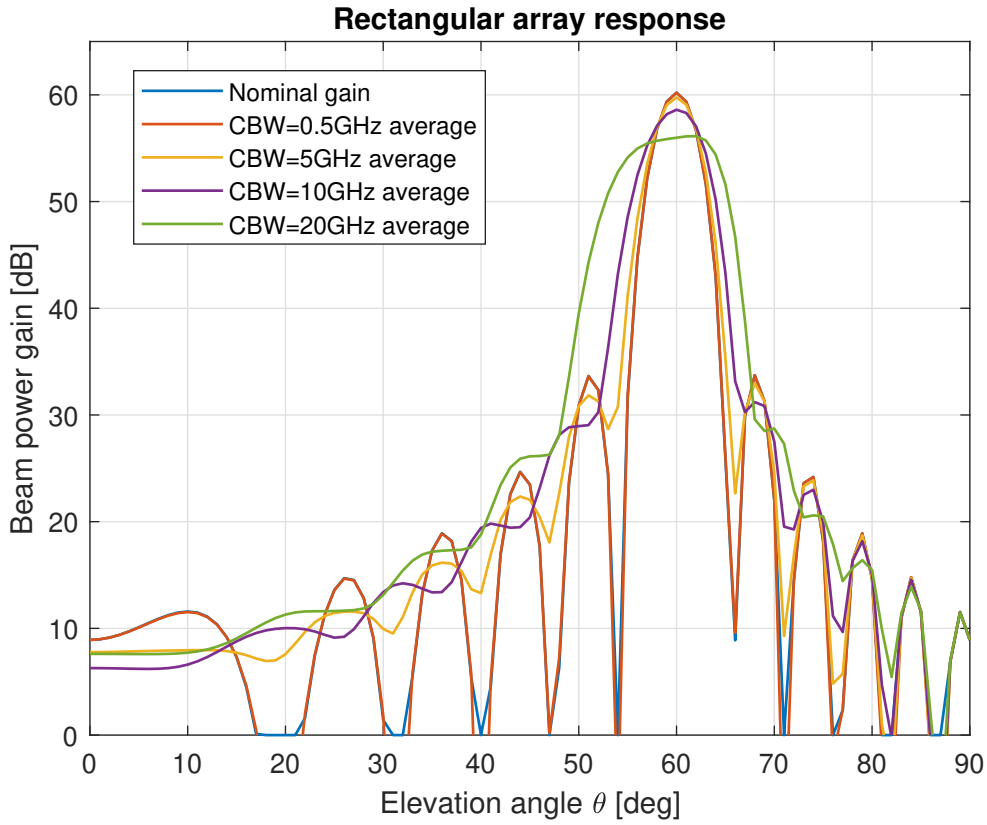

Figure 3.13. *Rectangular array response for UPA arrays with different channel bandwidths*

3.3 UCA

The uniform circular arrays are of extreme interest because their symmetrical geometry allows the phased antenna to scan towards the azimuth direction introducing small changes in terms of beam width and sidelobe level. Another characteristic of UCA is that they do not present edge elements and thus it is possible to rotate the radiation pattern electronically. The circular geometry is used also because it has the capability to compensate the effect of mutual coupling by breaking down the array excitation into a series of symmetrical spatial components [21].

Assuming the geometry depicted in 3.14, it is possible to consider that the wave is passing through the center at the time t=0, and it will cross *n*th element of the array at the relative time of [22]:

$$\tau_n = -\frac{a}{c}\sin\theta\cos\left(\phi - \phi_n\right) \tag{3.24}$$

where a is the radius of the array. In this case a positive time delay implies that the wave is impinging the nth antenna after crossing the center of the array, while a negative time delay implies that the wavefront impinged on it before arriving to the origin.

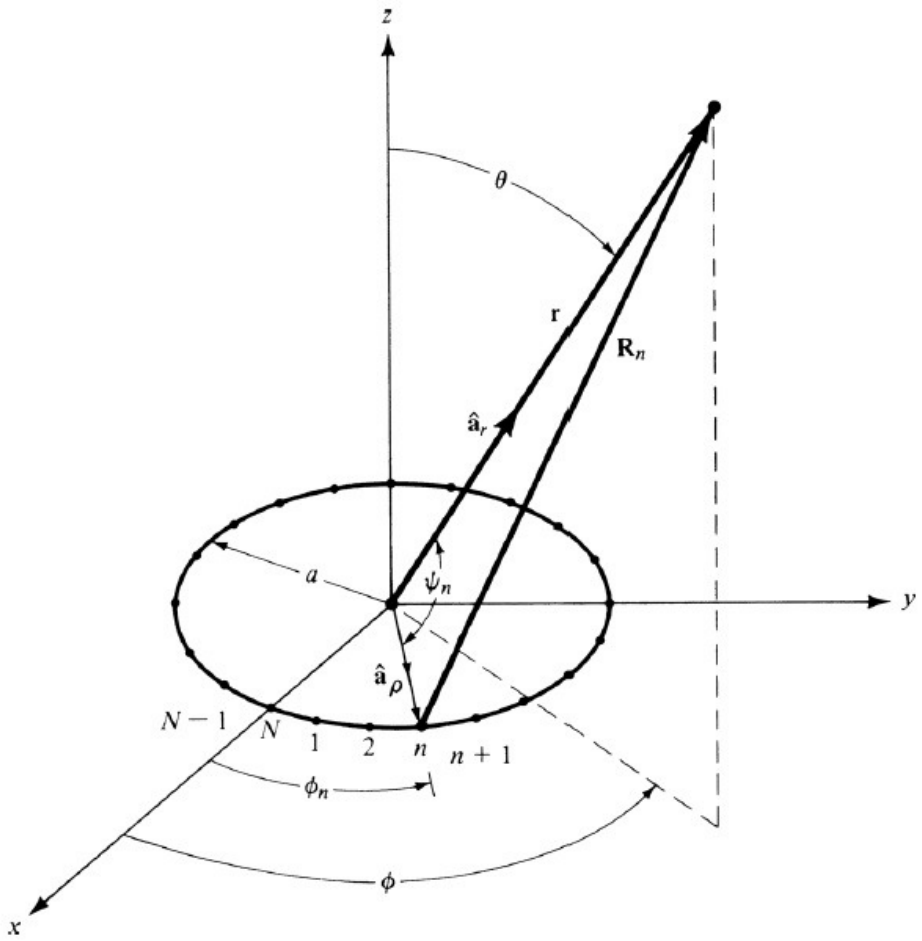

Figure 3.14. *Geometry of an N-element circular array [14]*

The expression of the steering vector of the uniform circular array was derived in [21] and has the following expression:

$$\mathbf{a}(\theta) = [e^{\varsigma \cos\phi - \phi_1}, e^{\varsigma \cos\phi - \phi_2}, \ldots, e^{\varsigma \cos\phi - \phi_n}] \tag{3.25}$$

where ς=$ka\sin\theta$ and **a(**θ**)** is used to represent source arrival direction.

More in general, the final expression of the sum of the received signals in very wideband systems where the time delay cannot be approximated, is given by:

$$R(f) = \sum_{n=1}^{N} e^{jka[\sin\theta\cos(\phi-\phi_n) - \sin\theta_0\cos(\phi_0-\phi_n)]} \sum_{n=1}^{N} e^{j2\pi f \tau_n} \tag{3.26}$$

As it was done for the previous arrays, in the next sections it will be analyzed how the different parameters are influencing the geometry response of the array both in the frequency and angular domain.

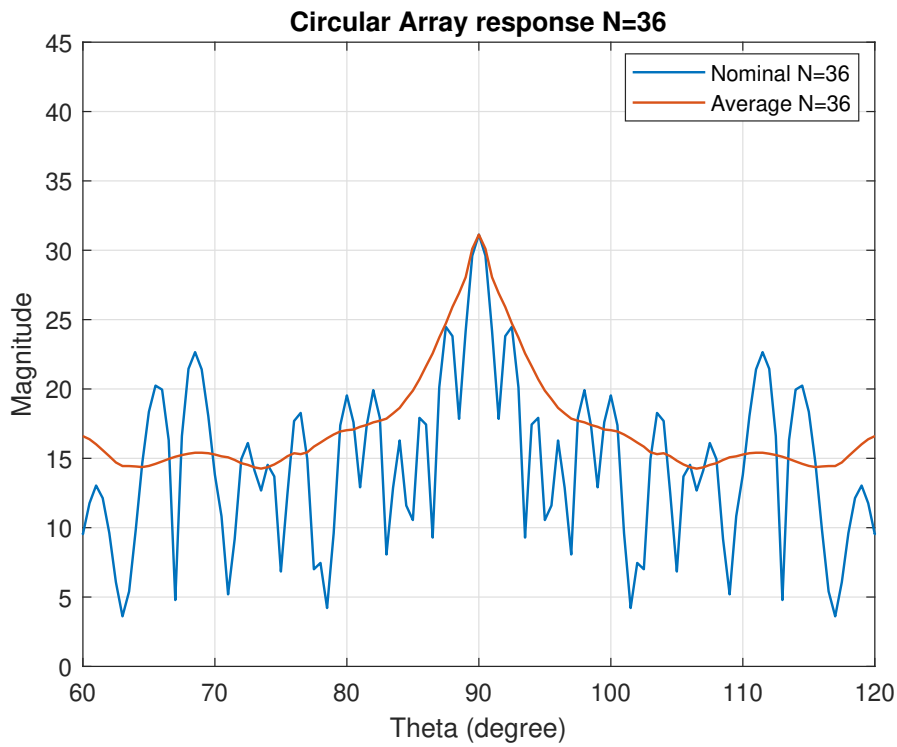

Figure 3.15. *Nominal and averaged plot for an array with 36 elements*

3.3.1 Different number of elements

As it was done in the previous sections for the linear and planar case, we are going to investigate how changes in the different parameters are influencing the array response of a circular array.

We first start by analyzing the changes due to a different number of elements in the array. In order to be able to compare the results with the ones obtained for ULA and UPA cases, the array was designed in such a way that it would occupy the same area of a UPA array with the same number of elements. All the simulations were done considering the circular array positioned on the xy-plane and a desired AoA exactly on the positive z-axis ($el = 90°$).

For the previous cases we noticed that the planar array was showing a better response under the beam squint phenomenon if compared to the linear one. In particular, the gain loss experienced was strongly decreased compared to the case of the linear array. The UCA configuration, instead, seems not to be affected at all by it. In fact, when considering a desired AoA perpendicular to the array surface there is no gain loss, which is an highly desirable characteristic.

On the other hand, as will be shown in the next section, when changing the AoA towards the plane where the array is positioned the effects caused by the beam will degrade in a very important manner the performance of the array.

The results are collected in 3.8: as mentioned before there is no gain loss when consid-

ering a radiation perpendicular to the array. Probably the circular array is not showing any gain loss because the maximum time delay between two elements is not so high compared to the one present between the first and last element in a ULA or UPA array. Moreover, also the $HPBW$ variation of the array is significantly decrease compared to the ULA and UCA cases.

3.3.2 Variations depending on AoA

More interesting results were obtained when studying the variation of the array response for different AoA. As for the case of planar array, it was important to notice that a change in the azimuth angle is not influencing at all the response of the array. In fact, this is one of the strength points of the circular array because its pattern is symmetric for all the azimuth angles. On the other hand, its response is strongly affected by the elevation angle. As we have seen in the previous section, the array response is perfect when considering a signal coming from the direction perpendicular to the array and the effect of beam squint. Unfortunately, even small variations from the perpendicular direction introduce big changes in the array pattern. In particular, a variation of $20°$ from the perpendicular direction is already enough for obtaining an array pattern which is not similar at all with the desired one. It means that the AoA will be shifted of several degrees and a huge gain loss will be present.Figure 3.16 is already showing the effects for an AoA with $el = 70°$.

Table 3.8. *Table of gain loss and HPBW variation depending on different number of elements for an UCA array*

$Number\ of\ elements$	$Gain\ Loss\ (dB)$	$HPBW\ variation$	$AoA\ (el)$
$N = 36$	1	0°	90°
$N = 128$	0	0°	90°
$N = 1024$	0	0°	90°

Table 3.9. *Table of gain loss and HPBW variation depending on different number of elements for an UCA array*

$AoA\ (el)$	$Gain\ Loss\ (dB)$	$HPBW\ av$	$HPBW\ nom$
$70°$	11.16	13.5°	1.5°
$80°$	8.53	11°	1.0°
$90°$	0	2°	1.0°

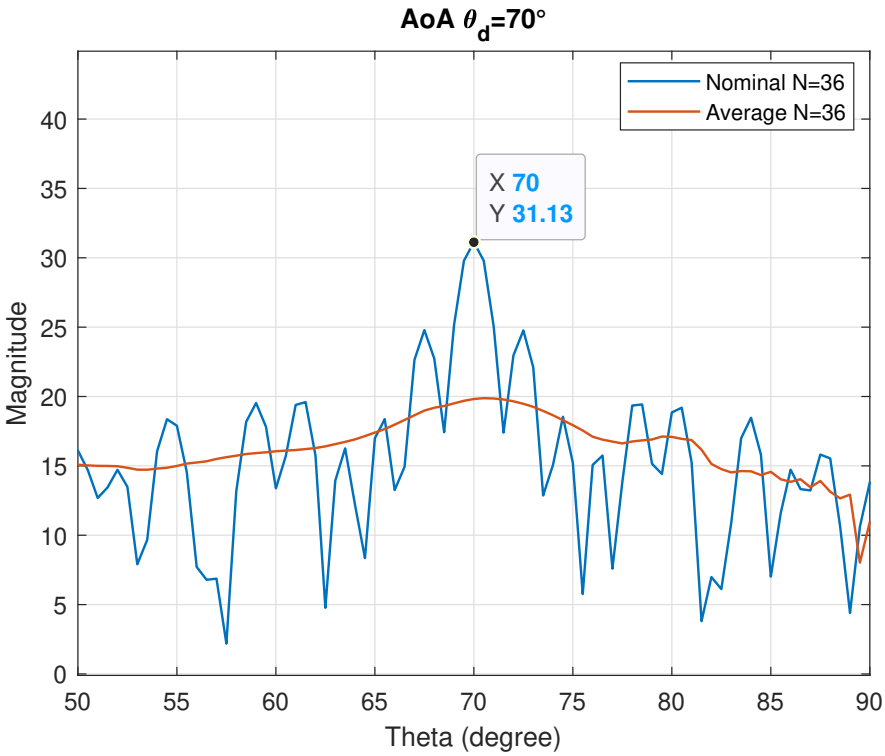

Figure 3.16. *Nominal and averaged plot for AoA with* $el = 70\,°$

Table 3.9 is showing us that the UCA response is influenced much more by the elevation angle. In fact, its results are characterized by an extremely high gain loss if we move of only few degrees from the z-axis. The planar array, instead, was presenting much lower gain loss even when considering AoAs very close to the xy-plane.

3.3.3 Variations depending on CBW

Finally, as last parameter, it was analyzed how the channel bandwidth is influencing the array response. Simulations were done utilizing an array of 128 elements, AoA perpendicular to the array and CBW respectively of 0.5, 5, 10 and 20GHz.

Also for this parameter the circular array showed a better response compared to the linear and planar ones when considering that the signal is coming from the direction perpendicular to the array. In fact, changing the channel bandwidth is not affecting at all the gain loss and the HPBW is not deteriorating so much. The results are collected in table 3.10.

Since the response for the array under beam squint phenomenon due to different channel bandwidths was almost perfect for AoA perpendicular to it, it was also decided to study how a different elevation angle would affect it. Thus, simulations with $el = 60\,°$ were made in order to compare it with the case studied in paragraph 3.2.3.

The patters obtained for the different CBWs are depicted in figure 3.17. As can be seen from the figure, the gain loss is very high if compared to the one obtained for the planar

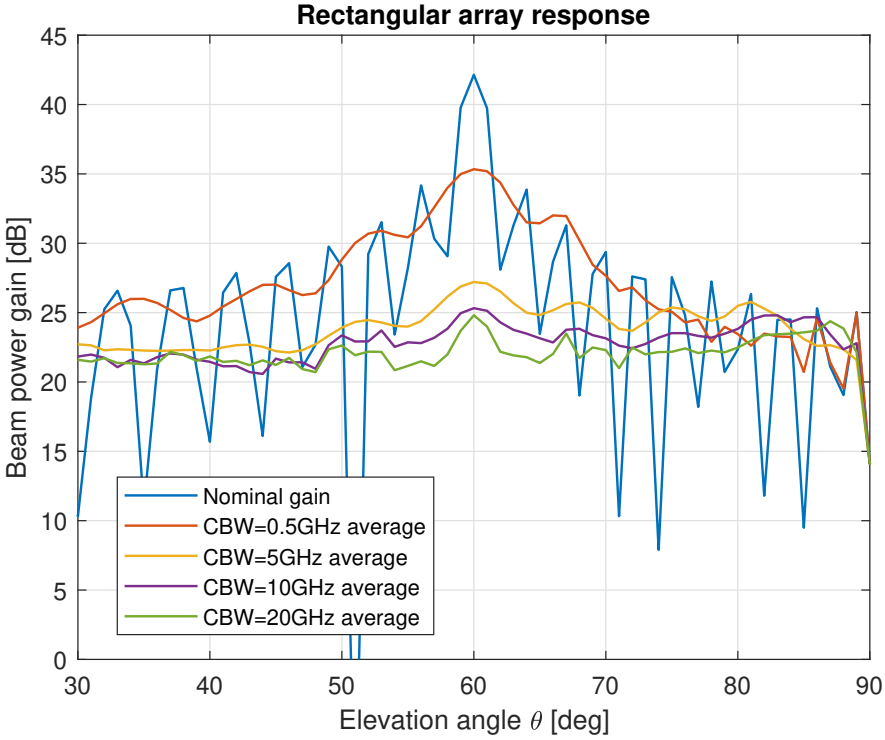

Figure 3.17. *Nominal and averaged plot for UCA array of 128 elements, with AoA* $el = 60\,°$ *and different CBWs*

array for the same elevation angle. This is really surprising because usually the circular configuration is preferred due to its symmetric characteristics while now it is showing an unexpected behaviour.

The results are collected in table 3.11. Comparing them with table 3.7 which was showing the same results for the planar case, we can see that there is an enormous difference between them. In fact, when using a circular array we have a gain loss of already $6.81dB$ for a CBW of only $0.5GHz$, which is higher than the gain loss experienced by a planar array with a CBW of $20GHz$. Moreover, it is also interesting to notice that the growth of the

Table 3.10. *Table of gain loss and HPBW variation depending on the channel bandwidth for an UCA array for AoA perpendicular to the array*

$CBW\ (GHz)$	$Gain\ Loss\ (dB)$	$HPBW\ av$	$HPBW\ nom$
$0.5GHz$	0	2°	2°
$5GHz$	0	2°	2°
$10GHz$	1	0°	2°
$20GHz$	4	0°	2°

channel bandwidth is causing an extreme dispersion of the main lobe for $CBW = 10GHz$, which results in an HPBW of $41.00°$. Obviously this is something we would like to avoid.

Table 3.11. *Table of gain loss and HPBW variation depending on the channel bandwidth for an UCA array for AoA with $el = 60\,°$ to the array*

$CBW\ (GHz)$	$Gain\ Loss\ (dB)$	$HPBW\ av$	$HPBW\ nom$
$0.5GHz$	6.81	8.00°	2°
$5GHz$	14.58	16.00°	2°
$10GHz$	15.61	41.00°	2°
$20GHz$	15.98	7.0°	2°

4 RADIO LINK SIMULATION AND RESULTS

In the previous chapter it was analyzed how the beam squint phenomenon is affecting the responses of different array geometries. The objective of this chapter is to link the theoretical results derived in chapter 3 with the effects caused by the beam squint phenomenon in an OFDM transmission link. In mm-Wave communications it is extremely important to choose the best path for the transmission due to the very high propagation losses, thus the beam squint phenomenon has to be taken into consideration when estimating the channel. The simulations in the previous chapter have shown that one of the main consequences of this problem is to introduce a frequency selectivity of the array response. Moreover, the current methods for estimating the channel are not considering any beam squint and this is increasing the channel estimation error which is the cause of the reduced capacity.

In this chapter we consider a a radio a link characterized by an analog beamforming architecture on the transmitter side, as it is shown in figure 2.10. The transmitting and receiving scheme utilized for the simulations are depicted in the figures 4.1 and 4.2:

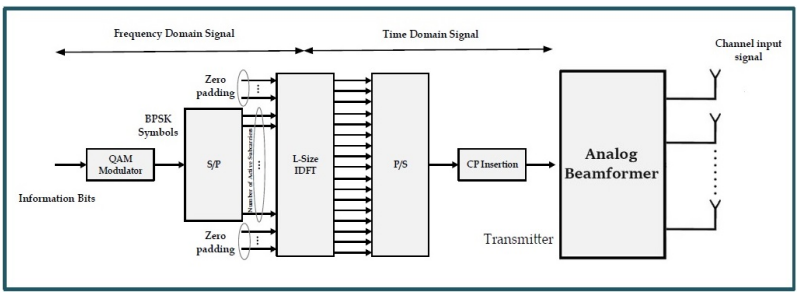

Figure 4.1. *Transmitter architecture with phased array*

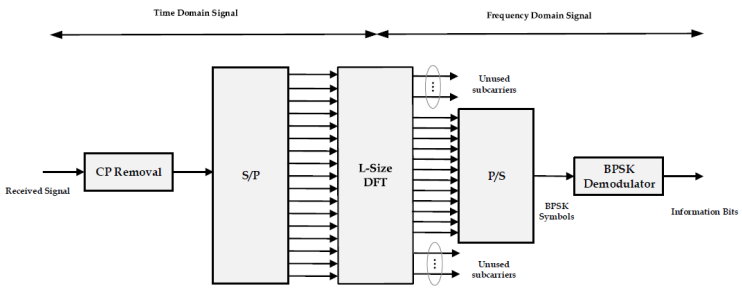

Figure 4.2. *Receiver architecture*

The communication is characterized by a carrier frequency of $fc = 65GHz$. In the communication we assume a number of 120000 active subcarriers with $15KHz$ carrier spacing. Such a big number of subcarriers is resulting in an available bandwidth of $1.8GHz$, which is a fairly value for the channel bandwidths available for communications over 60GHz. As can be seen form figure 4.1 the beamforming architecture consists of a phased array on the transmitter side and the beam squint phenomenon is modelled there. On the other hand, instead, the receiver is assumed to have only one antenna. Given the wavelength at this carrier frequency, and considering an element spacing equal to $\lambda/2$, the array is characterized by a total length of $0.37m$, which is an extremely small dimension if we consider that it is composed of 160 elements. This confirms the fact that it is possible to integrate a very high number of antennas in a limited area on a device. The transmit array was tuned to have his angle of departure in the direction of 30°. Due to the long dimension of the array compared to the sample duration, it was noticed that between the first and and last radiating element there was a delay of approximately 9 samples. This means that the signal transmitted from each antenna was delayed of $1/17$ of a sample if compared to the previous transmitting element.

The main challenge of this work came from the fact the the delays are substantially smaller than the sample duration of our simulator. Thus, it was need to apply some fractional delay filters to the propagating signal in order to see its effects. Since the signal was delayed of only a fraction of the sample duration, it was necessary to design a proper fractional delay filter which could simulate the desired delay. In particular, since every 17 antennas a signal is subject to a delay of one sample, it was necessary to design 10 fractional delay filters and to apply them in parallel.

In order to compare the results with the theory introduced in the previous chapter, we were interested in analyzing the spectra of the transmitted and received signals, which are shown in figures 4.4 and 4.5.

The simulations show that the behaviour of an array composed of 160 antenna elements with an available CBW of $1.8GHz$ are matching the results of figure 3.2. In fact, the power spectral density of the subcarriers at the extremity of the frequency band is showing

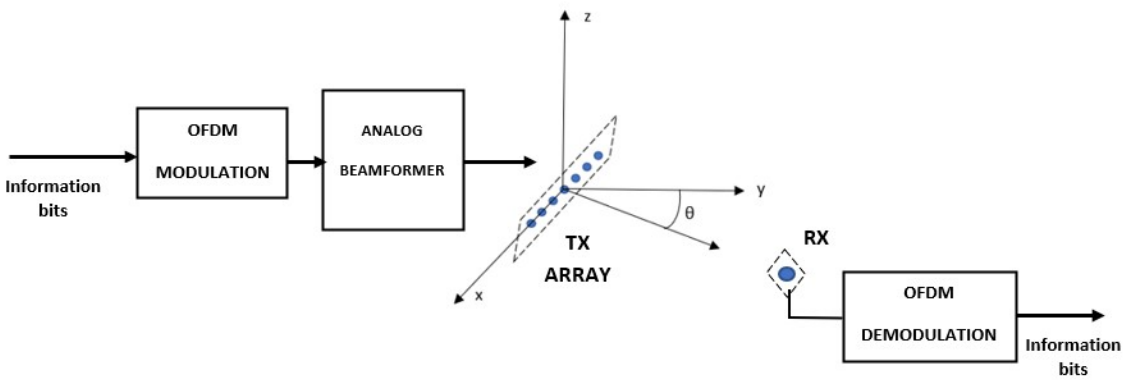

Figure 4.3. *System Geometry*

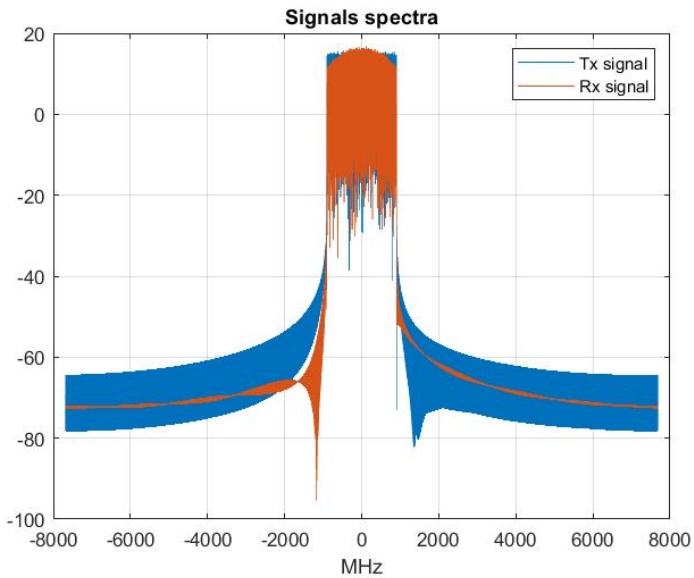

Figure 4.4. *Spectra of the transmitted and received signals in a communication characterized by the beam squint phenomenon*

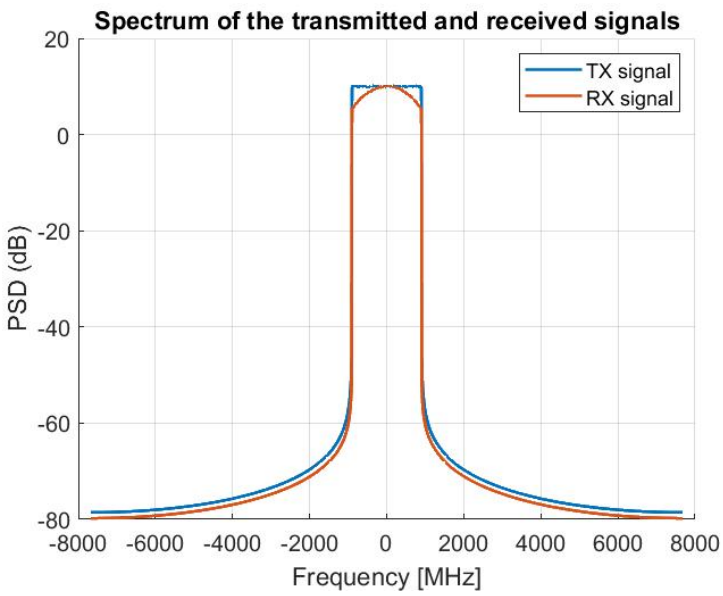

Figure 4.5. *Power spectral densities of the transmitted and received signals in a communication characterized by the beam squint phenomenon*

a loss of power, which is exactly what we were expecting to experience according to figure 3.2. In fact, the very large bandwidth of the signal and the very large dimensions of the array were generating a delay between the two ends of the array that was not negligible anymore if compared to the sample duration. This made the assumption of narrowband signal not to be valid anymore and is the exact interpretation of the beam squint phenomenon. In fact the delays have been modelled without approximating them with phase shifts and this made the received signal to be frequency dependent.

5 CONCLUSIONS

Beam squint is a concern for millimeter wave beamforming. In this thesis, one of the new challenges and problems that occur when working in the new frequency spectrum of millimeter waves is analyzed. It was shown that since the new generation technologies will utilize an higher frequency spectrum, their wavelength will be much smaller and thus more subjected to attenuation and to path loss. On the other hand, the smaller wavelengths will enable to reduce in a significant manner the dimensions of the antennas used in the array and thus, it will be possible to integrate an higher number of elements in the same area that was used before. This will improve the performances of the array resulting in an higher array gain. Nevertheless, the mm-wave communications are representing one of the most important topics regarding 5G technologies and they seem to be the best approach for LOS communications.

The problems deriving from utilizing very high frequencies make necessary to study and implement new techniques that will help to compensate for the higher losses. One of the main solution is represented by the beamforming. In chapter 2 the different architectures currently available were analyzed and it was pointed out that the best approach would be to used an hybrid configuration. The important characteristic of beamforming is that it will allow to increase in a consistent way the array gain in order to compensate for the path losses. The main benefit deriving from it is that it allows to create directional properties to the antenna system with fairly simple spatial signal processing. This will help to generate essentially a spatial filter, which will increase the spatial multiplexing gain of the transmission.

Since the 5G communication technologies will move towards an unexplored spectrum of frequencies, they will also be characterized by very wide bandwidths for the signals. In particular, since beamforming can be obtained by simply choosing accurately the phase and amplitude of each antenna element, this will influence the received signal at the array. In fact, the signals perceived at the elements which are on opposite sides of it will have time delays that will not allow them to combine coherently. This will make the narrowband approximation not to be valid anymore and thus it will imply a frequency dependency of the array response. This is the so called phenomenon of the beam squint.

In chapter 3 the beam squint phenomenon was modeled for different array geometries. In particular it was shown that it is depending on different parameters such as:

- Number of elements in the array

- AoA
- Channel bandwidth

Simulations have shown that a communication influenced by the beam squint phenomenon is experiencing a gain loss and a spread of the main lobe. It was demonstrated that, considering different array geometries with always the same number of elements, the linear array is the one experiencing an higher gain loss because of the higher delay difference between the antennas at his extremities. The simulations have shown an extremely interesting point for the UPA e UCA responses. In fact, these geometries are not changing their behaviour when the azimuth angle of arrival is changing.

Finally, we developed a channel model to conveniently capture wireless line of sight propagation as well as beam squint in a uniform linear array. Our study showed that beam squint can reduce channel capacity and increase channel estimation error. Therefore, system functions such as path selection or beam selection should also take beam squint into consideration. Generally speaking, the effects of beam squint on wireless system increase with the beam focus angle away from broadside, the number of antennas in the array or the fractional bandwidth.

This work provides a general overview and a fundamental study of beam squint in wireless communication systems. There remain a number of problems relating to beam squint that should be explored in the future, including but not limited to the following.

- Carrier Aggregation: it could be interesting to extend the carrier aggregation problem to UPA or other array geometries and to consider multiple paths within the main lobe in combination with carrier aggregation.
- Beamforming Codebook Design: it includes the problem of designing a set of beams, called a beamforming codebook, to cover a given range of AoA or AoD. The beams (codewords) in the codebook should meet some minimum performance requirements, such as minimum channel capacity or minimum array gain.
- Channel Estimation: it was shown that the beam squint is causing an increase in the channel estimation error and thus it could be interesting to study and implement new estimations algorithms that will be less influenced by it.

REFERENCES

[1] Ericsson Mobility report. (2019).

[2] Pi, Z. and Khan, F. An introduction to millimeter-wave mobile broadband systems. *IEEE Communications Magazine* 49.6 (2011), 101–107.

[3] Rangan, S., Rappaport, T. S. and Erkip, E. Millimeter-Wave Cellular Wireless Networks: Potentials and Challenges. *Proceedings of the IEEE* 102.3 (2014), 366–385.

[4] Zhang, J., Ge, X., Li, Q., Guizani, M. and Zhang, Y. 5G Millimeter-Wave Antenna Array: Design and Challenges. *IEEE Wireless Communications* 24.2 (2017), 106–112.

[5] Cai, M., Laneman, J. N. and Hochwald, B. Carrier Aggregation for Phased-Array Analog Beamforming with Beam Squint. *GLOBECOM 2017 - 2017 IEEE Global Communications Conference*. 2017, 1–7.

[6] Kutty, S. and Sen, D. Beamforming for Millimeter Wave Communications: An Inclusive Survey. *IEEE Communications Surveys Tutorials* 18.2 (2016), 949–973.

[7] *Why is the 60 GHz Band not good for long-range communications?* URL: https://www.everythingrf.com/community/why-is-the-60-ghz-band-not-good-for-long-range-communications (visited on 05/29/2020).

[8] Maccartney, G. R., Rappaport, T. S., Sun, S. and Deng, S. Indoor Office Wideband Millimeter-Wave Propagation Measurements and Channel Models at 28 and 73 GHz for Ultra-Dense 5G Wireless Networks. *IEEE Access* 3 (2015), 2388–2424.

[9] Sun, S., Rappaport, T. S., Thomas, T. A., Ghosh, A., Nguyen, H. C., Kovács, I. Z., Rodriguez, I., Koymen, O. and Partyka, A. Investigation of Prediction Accuracy, Sensitivity, and Parameter Stability of Large-Scale Propagation Path Loss Models for 5G Wireless Communications. *IEEE Transactions on Vehicular Technology* 65.5 (2016), 2843–2860.

[10] Samimi, M. K. and Rappaport, T. S. 3-D Millimeter-Wave Statistical Channel Model for 5G Wireless System Design. *IEEE Transactions on Microwave Theory and Techniques* 64.7 (2016), 2207–2225.

[11] Rappaport, T. S., Xing, Y., MacCartney, G. R., Molisch, A. F., Mellios, E. and Zhang, J. Overview of Millimeter Wave Communications for Fifth-Generation (5G) Wireless Networks—With a Focus on Propagation Models. *IEEE Transactions on Antennas and Propagation* 65.12 (2017), 6213–6230.

[12] Matolak, D. W., Remley, K. A., Holloway, C. and Gentile, C. Outdoor-to-Indoor Channel Dispersion and Power-Delay Profile Models for the 700-MHz and 4.9-GHz Bands. *IEEE Antennas and Wireless Propagation Letters* 15 (2016), 441–443.

[13] Balde, M. D., Vehmas, J., Nguyen, S. L. H., Haneda, K., Houas, H. and Uguen, B. A 32 GHz urban micro cell measurement campaign for 5G candidate spectrum

region. *2017 11th European Conference on Antennas and Propagation (EUCAP)*. 2017, 1803–1807.

[14] Balanis, C. A. *Antenna theory: analysis and design*. Wiley-Interscience, 2005.

[15] Stutzman, W. L. and Thiele, G. A. *Antenna Theory and Design*. John Wiley Sons, 2013.

[16] Cai, M. Modeling and Mitigating Beam Squint in Millimeter Wave Wireless Communication. (2018).

[17] Venkateswaran, V. and van der Veen, A. Analog Beamforming in MIMO Communications With Phase Shift Networks and Online Channel Estimation. *IEEE Transactions on Signal Processing* 58.8 (2010), 4131–4143.

[18] Lin, T., Cong, J., Zhu, Y., Zhang, J. and Ben Letaief, K. Hybrid Beamforming for Millimeter Wave Systems Using the MMSE Criterion. *IEEE Transactions on Communications* 67.5 (2019), 3693–3708.

[19] Heath, R. W., González-Prelcic, N., Rangan, S., Roh, W. and Sayeed, A. M. An Overview of Signal Processing Techniques for Millimeter Wave MIMO Systems. *IEEE Journal of Selected Topics in Signal Processing* 10.3 (2016), 436–453.

[20] Skolnik, M. I. *Introduction to Radar Systems /2nd Edition/*. 2nd ed. McGraw Hill Book Co., 1980.

[21] Noordin, N. H., Zuniga, V., El-Rayis, A. O., Haridas, N., Erdogan, A. T. and Arslan, T. Uniform circular arrays for phased array antenna. *2011 Loughborough Antennas Propagation Conference*. 2011, 1–4.

[22] Ioannides, P. and Balanis, C. A. Uniform circular arrays for smart antennas. *IEEE Antennas and Propagation Magazine* 47.4 (2005), 192–206.